Optimization of an Unfurlable Space Structure

Munira N. Sibai

Thesis submitted to the Faculty of the
Virginia Polytechnic Institute and State University
in partial fulfillment of the requirements for the degree of

Master of Science
in
Aerospace Engineering

Rakesh K. Kapania, Chair
Daisaku Inoyama
Gary D. Seidel
Mayuresh Patil

July 29, 2020
Blacksburg, Virginia

Keywords: Deployable structures, Unfurlable structure, Space structures, Structural optimization, Finite element analysis

Optimization of an Unfurlable Space Structure

Munira N. Sibai

(ABSTRACT)

Deployable structures serve a large number of space missions. They are vital since spacecraft are launched by placing them inside launch vehicle payload fairings of limited volume. Traditional spacecraft design often involves large components. These components could have power, communication, or optics applications and include booms, masts, antennas, and solar arrays. Different stowing methods are used in order to reduce the overall size of a spacecraft. Some examples of stowing methods include simple articulating, more complex origami inspired folding, telescoping, and rolling or wrapping. Wrapping of a flexible component could reduce the weight by eliminating joints and other components needed to enable some of the other mechanisms. It also is one of the most effective methods at reducing the compaction volume of the stowed deployable. In this study, a generic unfurlable structure is optimized for maximum natural frequency at its fully deployed configuration and minimal strain energy in its stowed configuration. The optimized stowed structure is then deployed in simulation. The structure consists of a rectangular panel that tightly wraps around a central cylindrical hub for release in space. It is desired to minimize elastic energy in the fully wrapped panel and hinge to ensure minimum reaction load into the spacecraft as it deploys in space, since that elastic energy stored at the stowed position transforms into kinetic energy when the panel is released and induces a moment in the connected spacecraft. It is also desired to maximize the fundamental frequency of the released panel as a surrogate for the panel having sufficient stiffness. Deployment dynamic analysis of the finite element model was run to ensure satisfactory optimization formulation and results.

Optimization of an Unfurlable Space Structure

Munira N. Sibai

(GENERAL AUDIENCE ABSTRACT)

Spacecraft, or artificial satellites, do not fly from earth to space on their own. They are launched into their orbits by placing them inside launch vehicles, also known as carrier rockets. Some parts or components of spacecraft are large and cannot fit in their designated space inside launch vehicles without being stowed into smaller volumes first. Examples of large components on spacecraft include solar arrays, which provide power to the spacecraft, and antennas, which are used on satellite for communication purposes. Many methods have been developed to stow such large components. Many of these methods involve folding about joints or hinges, whether it is done in a simple manner or by more complex designs. Moreover, components that are flexible enough could be rolled or wrapped before they are placed in launch vehicles. This method reduces the mass which the launch vehicle needs to carry, since added mass of joints is eliminated. Low mass is always desirable in space applications. Furthermore, wrapping is very effective at minimizing the volume of a component. These structures store energy inside them as they are wrapped due to the stiffness of their materials. This behavior is identical to that observed in a deformed spring. When the structures are released in space, that energy is released, and thus, they deploy and try to return to their original form. This is due to inertia, where the stored strain energy turns into kinetic energy as the structure deploys. The physical analysis of these structures, which enables their design, is complex and requires computational solutions and numerical modeling. The best design for a given problem can be found through numerical optimization. Numerical optimization uses mathematical approximations and computer programming to give the values of design

parameters that would result in the best design based on specified criterion and goals. In this thesis, numerical optimization was conducted for a simple unfurlable structure. The structure consists of a thin rectangular panel that wraps tightly around a central cylinder. The cylinder and panel are connected with a hinge that is a rotational spring with some stiffness. The optimization was solved to obtain the best values for the stiffness of the hinge, the thickness of the panel, which is allowed to vary along its length, and the stiffness or elasticity of the panel's material. The goals or objective of the optimization was to ensure that the deployed panel meets stiffness requirement specified for similar space components. Those requirements are set to make certain that the spacecraft can be controlled from earth even with its large component deployed. Additionally, the second goal of the optimization was to guarantee that the unfurling panel does not have very high energy stored while it's wrapped, so that it would not cause large motion the connected spacecraft in the zero gravity environments of space. A computer simulation was run with the resulting hinge stiffness and panel elasticity and thickness values with the cylinder and four panels connected to a structure representing a spacecraft. The simulation results and deployment animation were assessed to confirm that desired results were achieved.

Dedication

To my family-

Far or near, you kept me going

Acknowledgments

First and foremost, *Alhamdulillah*. All praise and gratitude is due to the Lord of our vast universe, the All-Knowing and Bestower of knowledge.

I would like to express my sincere gratitude to my advisor, Prof. Rakesh Kapania. I thank him for all he has taught me, and for his consistent feedback. Furthermore, this research collaboration between Virginia Tech and Northrop Grumman was born through his referral. I am also extremely grateful to my mentor at Northrop Grumman, Dr. Daisaku Inoyama, for guiding me through this research with his knowledge and experience.

Last and certainly not least, I would like to thank the director of Mechanical Analysis at Northrop Grumman Space Systems, Dr. Tom Stoumbos, for making this research possible through his continuous support and guidance.

Contents

List of Figures

List of Tables

Chapter 1

Introduction

1.1 Background and Motivation

Deployable structures serve many space missions. They are vital since spacecraft are launched by placing them inside a launch vehicle payload fairing of limited volume. Traditional spacecraft design often involves large components. These components could have power, communication, or optics applications and include booms, masts, antennas, and solar arrays. Different stowing methods are used to reduce the overall size of a spacecraft. Some examples of stowing methods include simple articulating, more complex origami inspired folding, telescoping, and rolling or wrapping.

Wrapping of a flexible component could reduce the weight by eliminating joints and other components needed to enable some of the other stowing mechanisms. It also is one of the most effective methods at reducing the compaction volume of the stowed deployable. Large flexible components, such as antennas and solar arrays can be stowed by wrapping. They are then released for deployment in space due to their own stored elastic energy. It is important to design the component for successful deployment, while also ensuring that the structure does not impart excessive reaction load into the spacecraft as it unfurls. Additionally, to ensure control of the spacecraft system is maintained, deployed space components need to satisfy stiffness requirements.[18]

In this research, numerical methods were used in order to obtain an optimal design of a generic unfurlable structure consisting of a long thin panel and a central cylindrical hub. The objective of the research was to cultivate an understanding for the underlying analysis and behavior of this type of deployable structures, and subsequently develop an optimization formulation and approach. The simple structure was selected as a representation of potential, more complex unfurlable structures. The panel of length L, height H, and thickness t is wrapped tightly around the center cylindrical hub, and then released to deploy. The panel is connected to the hub with a hinge of rotational stiffness k. The dimensions of the hub were chosen to be smaller than typical launch vehicle payload fairing volume. The length of the panel was also selected as a representation of appropriate flexible deployable structures. Those dimensions are shown in Fig. 1.1.

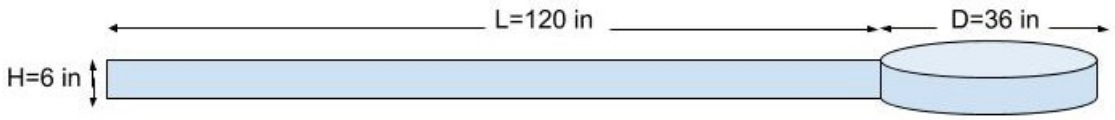

Figure 1.1: Schematic of deployed unfurlable structure

The structure was optimized by solving for hinge stiffness, panel elastic modulus and panel thickness that maximizes natural frequency at its fully deployed configuration and minimizes strain energy in its stowed configuration. It is desired to minimize the elastic energy in the fully wrapped panel and hinge in order to ensure minimum reaction load into the spacecraft as it deploys in space. Moreover, maximizing the fundamental frequency of the released panel is necessary as a surrogate for the panel having sufficient stiffness.

The optimization was solved for a finite element model of the hinge and panel with non-uniform thickness. In order to verify the finite element model, the closed-form solution for elastic energy and fundamental frequency were obtained assuming a uniform panel. Further-

more, these solutions served for a better understanding of the dependency and sensitivity of the objectives to the design variables. Contours of the objective functions with respect to the design variable were plotted for the uniform panel. Optimization was solved using both Sequential Quadratic Programming (SQP) and Archive based Mirco Genetic Algorithm (AMGA) for different objective weights and formulations. Finally, deployment dynamic analysis of the finite element model was run for optimized stowed structure to ensure satisfactory optimization formulation and results.

1.2 Optimization Problem Formulation

Two objective functions were considered here. The first objective of the optimization was to keep the reaction moment in the spacecraft due to deployment minimal. This was achieved through minimizing the elastic strain energy of the fully wrapped panel added to the elastic energy in the hinge at that fully stowed position. The second objective was to attain stiffness requirement. Thus, the fundamental frequency, f_n, of the hinge and panel was maximized. The multi-objective optimization was completed for different weights, α_1 and α_2, and the results were compared. The optimization was also run for two different objective function formulations as shown in Eq. 1.1 and Eq. 1.2.

Minimize:

$$f_{objective} = \alpha_1 \, f_1(E,k,t) - \alpha_2 \, f_2(E,k,t) \tag{1.1}$$

or

$$f_{objective} = \alpha_1 \, f_1(E,k,t) + \frac{\alpha_2}{f_2(E,k,t)} \tag{1.2}$$

where,

$$f_1 = Elastic\, Energy(E,k,t) \tag{1.3}$$

$$f_2 = f_n(E, k, t) \tag{1.4}$$

The design variables of the optimization problem were the elastic modulus of the panel, E, the thickness of each element of the panel, t, and the stiffness of the hinge, k. Having the panel's modulus of elasticity as a design variable translates the solution into a material choice, while thickness represents the geometry. In terms of a laminate composites, defining elasticity and thickness independently enables the selection of materials, as well as ply count, thickness, and orientation. The two objective functions terms are contradictory since they are both directly proportional to all design variables. Thus, optimal balance is sought while staying within constraints. The constraints were specified for each design variable to keep it within reasonable limits of available and appropriate materials, reasonable structure size and mass, and functional hinges. The upper and lower bound for thickness and elastic modulus were chosen based on the quasi-isotropic properties of a commonly used laminate material, where the total thickness and equivalent elastic modulus were calculated for a maximum and minimum number of plies. The lower bound was specified for 4 plies, each with a thickness of 0.0025 in, while upper bound corresponds to 12 plies of the laminate material. The panel thickness and elastic modulus constraints are given by Eq. 1.5 and Eq. 1.6 respectively.

The lower bound of the hinge's rotational stiffness was specified to be 1 lb.in/rad through analysis. This value was chosen since it is the lowest stiffness value that satisfies $f_n \geqslant 0.01$ Hz for a panel with the lower bound of thickness and elasticity. The 0.01 Hz minimum fundamental frequency is a reasonable requirement for a slender space deployable. An upper bound for the hinge stiffness was also specified as 100 lb.in/rad. The hinge stiffness constraint is given by Eq. 1.7. A stress constraint was also specified for the panel. The maximum allowed stress was based on the tensile strength of the aforementioned laminate material with a factor of safety of 1.5, as shown in Eq. 1.8 [28].

$$0.01 \leqslant t \leqslant 0.03\ in \tag{1.5}$$

$$2.5\ E\ 6 \leqslant E \leqslant 1\ E\ 7\ psi \tag{1.6}$$

$$1\ \leqslant k \leqslant 100\ lb.in/rad \tag{1.7}$$

$$\sigma \leqslant \frac{\sigma_{Composite\ Tensile\ Strength}}{Factor\ of\ Safety} = \frac{370\ ksi}{1.5} = 250\ ksi \tag{1.8}$$

An additional optimization run also included a mass constraint, namely, the total mass of the panel was bounded to a maximum of 70 percent of the mass at upper bound of the thickness constraint. The density of a commonly used material in aerospace applications was assumed for the panel in this project. The mass constraint is given by Eq. 1.9.

$$m \leqslant 0.7 \times \rho\ H\ L\ t_{max} = 1.47\ lbs \tag{1.9}$$

The optimization problem was formulated to guarantee the functionality and controllability of the deployable structure and connected spacecraft, by ensuring sufficient stiffness and low moments and stresses, all of which are critical to the success of a spacecraft's mission. In the next chapter, literature on deployable structures is discussed. Reviewing literature provided an insight to the need for this study as well as a better understanding of the applications and physics of these structures.

Chapter 2

Literature Review

Deployable structures are widely employed in space applications since large space components need to be stowed before they are launched. By the nature of some applications, such as optic missions, larger apertures are generally better[20]. Subsequently, there is a fair amount of literature on the design and analysis of these assemblies. In order to explore the need and applicability of the presented research, and to learn more about the design and applications of deployable structures, a literature review was conducted. Multiple literature investigates different stowing and deployment methods or list the ongoing developments in deployable structures design. Others present novel techniques and geometries. Some involve dynamic analysis or test results or focus on stiffness and damping specifications. Although there is extensive literature on deployable structures, very few of those are on structural optimization. This review focuses on information in literature that is relevant to this thesis.

A paper on deployable structures by Del Grosso and Basso defines them by stating that "The generic name deployable structures is used for a broad category of structures that can be transformed from a closed compact configuration to a predetermined expanded form, in which they are stable and can carry loads."[5]. The paper classifies deployable structures as a special case within the category of adaptive of morphing structure, where, generally, the focus is on the change of shape between only two configurations: the initial compact configuration and the final deployed one. Another study that evaluates the performance of deployable

structures numeric simulations states that these structures are deployed in space by means of both the release of stored strain energy and motor actuation through gears, linkages, or cables [16]. The deployment of the structure optimized in this thesis is achieved through the energy stored in the stowed panel and stowed hinge alone, and no motor actuation is involved. Del Grosso et al. state that many technical solutions and human actions can be used for the actuator systems of a deployable structure, while the structural component is where the main design challenges are.

Kiper and Soylemez investigated various designs of deployable structures, focusing on their geometry[9]. The paper mentions that, according to Salama et al., space systems experience their highest failure rate during deployment, and typically perform well after they are properly deployed[21]. Thus, design and analysis of deployable structures is of great importance. Kiper et al. states that deployable structures are used to make transportation possible by keeping the structure compact during launch, or when adaptability of shape or function is needed.

Kiper et al. distinguishes between rigid and flexible assemblies. They define rigid assemblies as those involving rigid elements connected with rigid joints. The advantages of rigid assemblies are shape control, while some of their disadvantages are complexity of parts, added weight, friction in joints, and in some cases, the high cost of parts and assemblies. On the other hand, flexible assemblies may or may not incorporate any rigid parts. It was noted while surveying literature on deployable structures for this thesis that most of them were on rigid structures that deploy about joints, such as umbrella-like antennas, and telescoping masts. There is not as much literature on flexible deployables. The research in this thesis looks at an entirely flexible panel, except for hinge connecting the panel to the central hub. Kiper et al. goes on to say that flexible structures generally consist of simple structures but pose difficulty in design and shape accuracy and control. Furthermore, the section on

antennas in Kiper et al.'s paper mentions that, according to Lake et al., the larger the size of an antenna, the more involved and costly the design will be [11]. This thesis aims to alleviate the design process of a large, flexible deployable structure by developing a novel method for its optimization.

The literature reviewed on examples of deployable structure showed that typical spacecraft structures have lightweight components in deployed configuration especially designed for space. Testing on the ground does not accurately represent their behavior in space. Ground testing is also difficult and unmanageable because of the sensitivity of these structures to friction, gravity, and air drag, especially with larger structures. Thus, such structures are studied and verified by a combination of component level testing and analytical simulations. This shows how crucial accurate analytical simulation is for large deformation deployment structures. This includes damping definition which plays an important role in deployment dynamics. Optimizing such structures simplifies the design process of these highly complex structures. Some deployable structure presented in literature have a similar mechanism to the structure optimized in this thesis. Those include a roll-out solar array and unfurlable antenna, both of which were developed by Lockheed Martin, and the starshade occulter of NASA's Habitable Exoplanet Observatory (HabEx).

In a study by Winter et al., the PowerSail roll-out solar array is presented[27]. The array is similar to the structure studied in this thesis in that it is flexible, stowed by wrapping, and depthless. Winter et al's paper mentions that this structure is fitting for solar array applications since a primary driver of the design is the mass, and this type of deployable is highly effective at mass reduction. Additionally, the authors state that the roll out mechanism is suitable for solar array even though mass reduction comes at the expense of rigidity since power-generation capability is not highly affected by increased dynamics. The deployment of the solar array was enable by the use of shape memory longerons and transverse composite

tensioning members. In contrast to the deployment simulation presented in later chapters of this thesis, which did not involve temperature variation, the shape memory actuators of the roll-out PowerSail were heated to facilitate unwrapping at a controlled rate and to enable the locking of the array into a fully deployed structure of relatively high stiffness.

A study on Lockheed Martin's wrap-rib antenna design was conducted by Wade, Sinha and Singh[23]. The authors present an overview of the geometry and design approach of the unfurlable antenna. The antenna consists of multiple curved cantilever ribs, each connected to a central hub by a hinge. The ribs are made of a composite laminate of a graphite epoxy material and have a lenticular cross-section which enables the elastic buckling and flattening when the ribs are wrapped around the central hub. Sewn to the ribs are gores made from a fabric of electrically conductive material that from a flexible membrane. Wade et al.'s paper mentions that the symmetric parabolic construction resulting from the curved shape of the ribs of the wrap-rib antenna is the most comment construction for large antenna, and that the design becomes closer to a true paraboloid of revolution as the number of gores is increased. In order to achieve that final shape, the structure is deployed by a restraint mechanism that helps in controlling the deployment rate by controlling the rate of energy release. That mechanism basically consists of a motor-driven reel-to-reel tape drive that interacts with the ribs as they unfurl.

Another example of a unfurlable space component is discussed in an interim report on NASA's Habitable Exoplanet Observatory (HabEx) [6]. The report presents potential designs for the deployable occulting starshade of the proposed observatory. The starshade is to fly in formation with the HabEx telescope with the purpose of creating a deep shadow that suppresses light from a patent star to reveal the reflected light from exoplanets in that star's system. One of the proposed designs include furled petals, the design of which has been developed by Jet Propulsion Laboratory since 2010. The unfurlable petals are one of

the two subsystems incorporated in the suggested design. The design consists of an inner disk that is the core of the structure on which the petals attach. The starshade and telescope are shown in Fig. 2.1. The inner disk deploys independently following the outer petals unfurling stage and is driven by perimeter trusses. Figure 2.1(a) shows the petals as they are unfurling, and Fig. 2.1(b) shows the fully deployed starshade after the inner disk in also deployed. The report references the Lockheed Martin wrap-rib approach, which resulted in successful on-orbit deployment for hundreds of times, as the basis for the proposed petal deployment approach. To deploy the stareshade, the preload mechanism used to stow the structure is released, and the petals stored strain energy leads them to press lightly against a motor-driven roller assembly. That assembly is designed to control dynamic excitation to protect the petals from damage.

The aforementioned wrap-rib antenna, PowerSail roll-out solar array and proposed HabEx starshade show that unfurlable structures can be applied to a wide range of existing and future space components. All of those examples employ mechanisms to restrain the deployment. The optimization done in this thesis aims to improve controllability of the deployment solely though the reduction of the stored energy in the wrapped panel. The unfurling simulation of multiple panels discussed in a later chapter also included some axial stiffness and damping between each of the panels.

A study done on a large antenna with flexible booms over 780 inches long was conducted by Mobrem and Adams[15]. The paper discusses the deployment of the lenticular booms that form the antenna onboard the Mars Express spacecraft (MARSIS), developed and built by Northrop Grumman Space Technology Astro Aerospace. MARSIS spacecraft with its antenna deployed is illustrated in Fig. 2.2. Mobrem et al.'s research suggested the importance of optimizing strain energy of such structures in future work so that it is not too large as to result in violent deployment, but large enough to ensure successful and complete deployment.

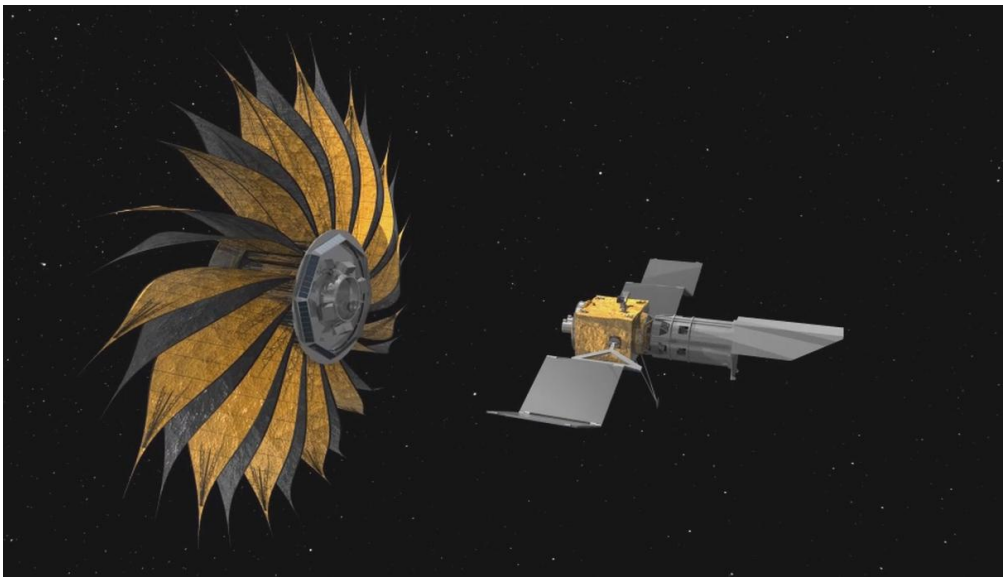

(a)

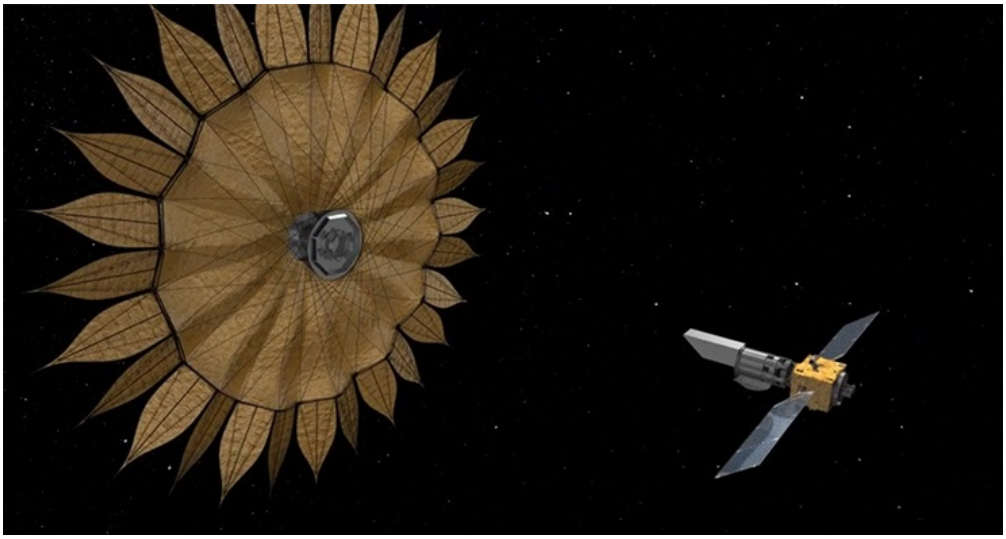

(b)

Figure 2.1: HabEx telescope and starshade (a)during deployment (b)after fully deployed [17]

A study where a deployable structure was optimized similarly to this thesis was done by Kwak et al. on the shape optimization of a deployable antenna reflector[10]. The shape of the reflector was optimized to satisfy stiffness requirements, while minimizing weight. The antenna optimized in the study consisted of multiple curved ribs that wrap around a central hub in a near-vertical configuration. The panel studied in this thesis is more

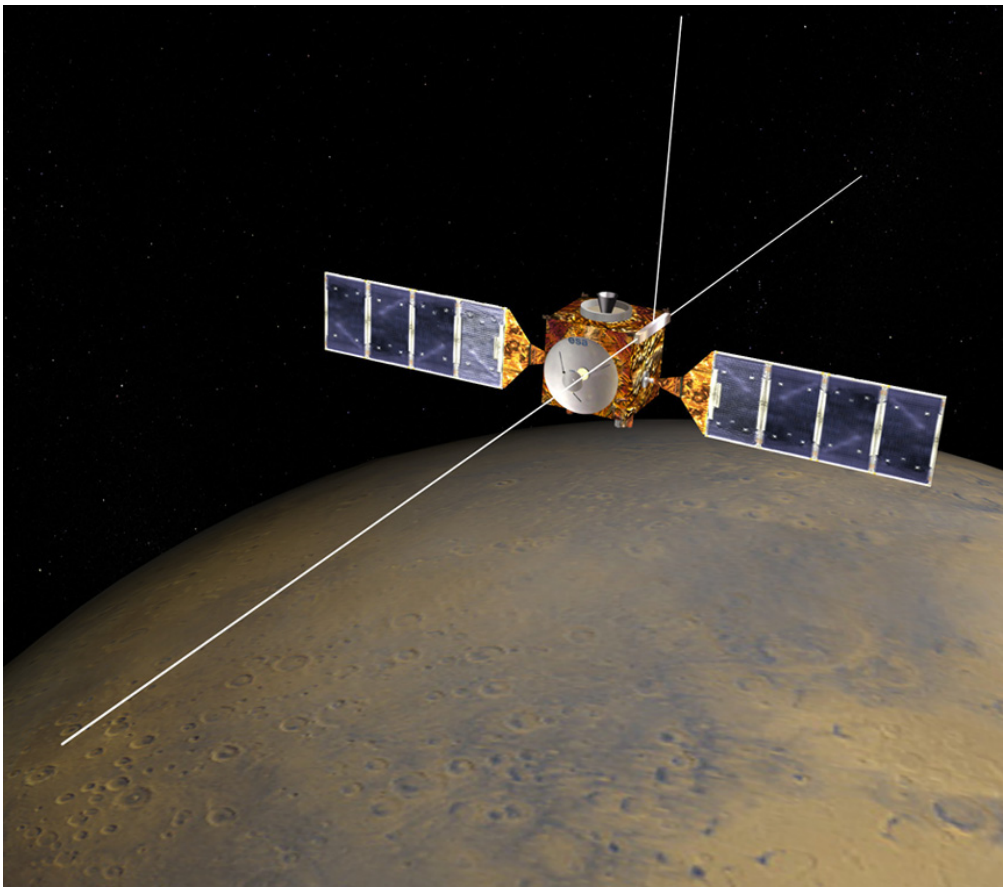

Figure 2.2: Illustration of MARSIS spacecraft with fully deployed booms [24]

generic, and the devised optimization method is applicable to flexible unfurlable structures beyond antennas. Additionally, the optimization presented in this thesis consists of a multi objective optimization that includes, in addition to the stiffness objective, the minimization of the strain energy stored in the wrapped system. Furthermore, Kwak et al. explored the materials and elastic modulus through analysis and conducted the optimization for the shape, while the modulus of elasticity in this thesis was specified based on numerical optimization, in addition to the non-uniform thickness of the panel.

Chapter 3

Methods of Analysis and Optimization

3.1 Analysis of a Uniform Panel

The closed-form solutions for elastic energy and fundamental frequency were obtained for a hinged panel of uniform thickness. These equations were then solved for a specific value of panel thickness, modulus of elasticity and hinge stiffness, and the results were compared to the finite element models with the same parameter values for verification. Additionally, the closed-form solution for stress in the panel -a constraint of the optimization- was obtained in terms of thickness and stiffness. Contours of the closed-form solutions were plotted for each set of two design variables. The contours were plotted for the upper bound, lower bound, and mid-value of third design variable. The plots gave valuable insight about the dependency and sensitivity of the objectives to the design variables.

3.1.1 Closed-Form Solutions

First, the closed-form solution for the elastic energy objective was acquired. The strain energy stored in the wrapped panel and the elastic energy in the hinge at the stowed position transforms into kinetic energy when the panel is released and induces a moment in the

connected spacecraft. This could result in undesirable motion in a space environment. Thus, it is important to minimize the energy to ensure controlled deployment of the panel and minimal moments into the spacecraft. The hinge is modeled as a rotational spring and its potential energy is given by Eq. 3.1. Strain energy in the wrapped panel, shown in Eq. 3.2, depends on the curvature of the cylindrical hub, κ, the Young's modulus of the panel, E, and the area moment of inertia of the panel, I, which depends on the design variable t. The objective function consists of these two energy values combined, as shown in Eq. 3.3 [8].

$$U_{hinge} = 0.5\, k\, \theta_{hinge}^2 \tag{3.1}$$

$$U_{panel} = \int_0^L 0.5\, M\, \kappa\, dx = \int_0^L 0.5\, EI\, \kappa^2\, dx \tag{3.2}$$

$$U = U_{hinge} + U_{panel} = 0.5\, k\, \theta_{hinge}^2 + \int_0^L 0.5\, EI\, \kappa^2\, dx \tag{3.3}$$

The moment of inertia of the thin rectangular panel is $\frac{1}{12}Ht^3$, where the height, H, equals 6 inches. The cylindrical hub around which the panel wraps is 18 inches in diameter. Since the panel wraps tightly around the hub, its curvature when stowed will be the reciprocal of the radius. The panel is normal to the hub at the fully deployed configuration. When the panel is stowed the rotation angle of the hinge will be 90 degrees, in other words, the hinge maximum rotation is when the panel is tangent to the hub. Substituting in the values for hinge rotation angle, panel curvature, and the panel's moment of inertia, we get the total elastic energy in the stowed panel and hinge in terms of the design variables given in Eq. 3.4. For a uniform thickness, we solve the integral for the total length of 120 inches to get Eq. 3.5.

$$U = \frac{\pi^2}{8}\, k\, + \int_0^L \frac{E\, t^3}{1296}\, dx \tag{3.4}$$

$$U = \frac{\pi^2}{8}\, k \, + \frac{5}{54}\, E\, t^3 \tag{3.5}$$

The natural frequency problem was solved for a uniform beam that is free on one end and connected to both a rotational and a linear spring on the other end, as shown in Fig. 3.1. The linear spring is semi-rigid with a high stiffness value equal to $1{\times}10^7$ lb/in, restricting the panel's vertical deflection. Using Euler-Bernoulli beam theory is appropriate for our panel since the ratio of the panel's length to its depth is relatively large and is equal to $\frac{L}{H} = \frac{120}{6} = 20$. Thus, we can write the partial differential equation for bending vibration of a beam as shown in Eq. 3.6. For a beam with uniform mass, modulus of elasticity and inertia, that equation simplifies to Eq. 3.7 [14].

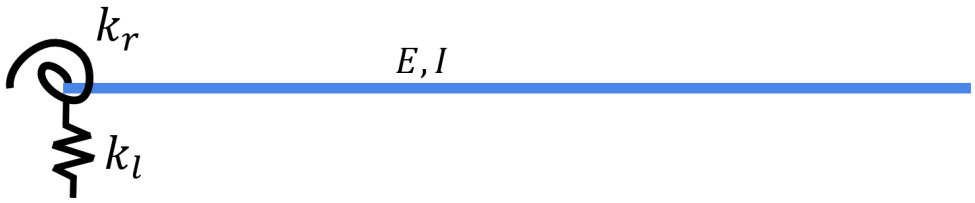

Figure 3.1: Schematic of beam boundary conditions

$$-\frac{\partial^2}{\partial x^2}[EI(x)\frac{\partial^2 y(x,t)}{\partial x^2}] + f(x,t) = m(x)\frac{\partial^2 y(x,t)}{\partial t^2},\ 0 < x < L \tag{3.6}$$

$$-\frac{d^4 Y(x)}{dx^4} - \beta^4\, Y(x) = 0 \tag{3.7}$$

where,

$$\beta^4 = \frac{\omega^2 A \rho}{EI} \tag{3.8}$$

The solution to the forth order differential equation is given by Eq. 3.9. The differential equation was solved for the boundary conditions presented in Eqs. 3.10 - 3.13 [4]. The result-

ing characteristic equation is given in Eq. 3.14. In order to obtain the value of fundamental frequency, the first root of the characteristic equation was found numerically for a given set of parameters.

$$Y(x) = A\,sin(\beta x) + B\,cos(\beta x) + C\,sinh(\beta x) + D\,cosh(\beta x) \tag{3.9}$$

Shear Force at hinge end ($x = 0$):

$$\frac{d^3Y(x)}{dx^3} = \frac{k_l}{EI}Y(x) = \frac{1 \times 10^7}{EI}\,Y(x) \tag{3.10}$$

Moment at hinge end ($x = 0$):

$$\frac{d^2Y(x)}{dx^2} = \frac{k_r}{EI}\frac{dY(x)}{dx} \tag{3.11}$$

Shear force at free end ($x = L$):

$$\frac{d^3Y(x)}{dx^3} = 0 \tag{3.12}$$

Moment at free end ($x = L$):

$$\frac{d^2Y(x)}{dx^2} = 0 \tag{3.13}$$

$$\begin{aligned}&\frac{-2}{(EI)^2}[1 \times 10^7 k - (EI)^2\beta^4 + cosh(L\beta) \times [(1 \times 10^7)k + (EI)^2\beta^4)cos(L\beta) + \\ &EI\beta(-1 \times 10^7 + k\beta^2)sin(L\beta)] + EI\beta(1 \times 10^7 + k\beta^2)cos(L\beta)sinh(L\beta)] = 0\end{aligned} \tag{3.14}$$

Lastly, the solution for the stress constraint in terms of the panel design variables was obtained. The stress in the fully wrapped panel is given by Eq. 3.15, where M is the internal bending moment in the panel and c is the distance to the neutral axis, which is at the center of the thickness. The solution in terms of E and t shown in Eq. 3.15 was obtained

by substituting in the values of curvature and height. Stress for the upper bounds of E and t is $8,300$ psi, which is well below the maximum allowed value of 250 ksi. Therefore, the constraint is not active for any possible solution of the optimization of the panel in the stowed configuration.

$$\sigma = \frac{Mc}{I} = \frac{EI\kappa\, t}{2I} = \frac{Et}{36} \tag{3.15}$$

3.1.2 Objective Functions Contour Plots

The objective function terms were plotted separately in two-dimensional contour plots for a uniform panel. They were plotted for each combination of two out of the three design variables. Graphs were obtained at values of the third design variable corresponding to the upper bound, lower bound and middle value of its allowed range. The graphs are presented here.

For the elastic energy of a uniform beam, Fig. 3.2 shows that the value of the strain energy in the panel added to the elastic energy of the hinge depends largely on the value of k, as opposed to its dependency on E. It can also be concluded that the thicker the panel, the larger the influence of its elastic modulus on the value of elastic energy. The close values of elastic energy for each of the three contour plots also show the small dependency on the thickness of the panel. This makes sense since the allowed values of t are below 1, and thickness is cubed in the elastic energy function presented in Eq. 3.5. The small dependency on E can also be inferred from the energy function for a hinged uniform beam, since the factor multiplying k in the hinge energy term is larger than that of E in the panel energy term. The value of elastic energy is directly proportional to all design variables.

The plots shown in Fig. 3.3 allow us to compare the sensitivity of the elastic energy value

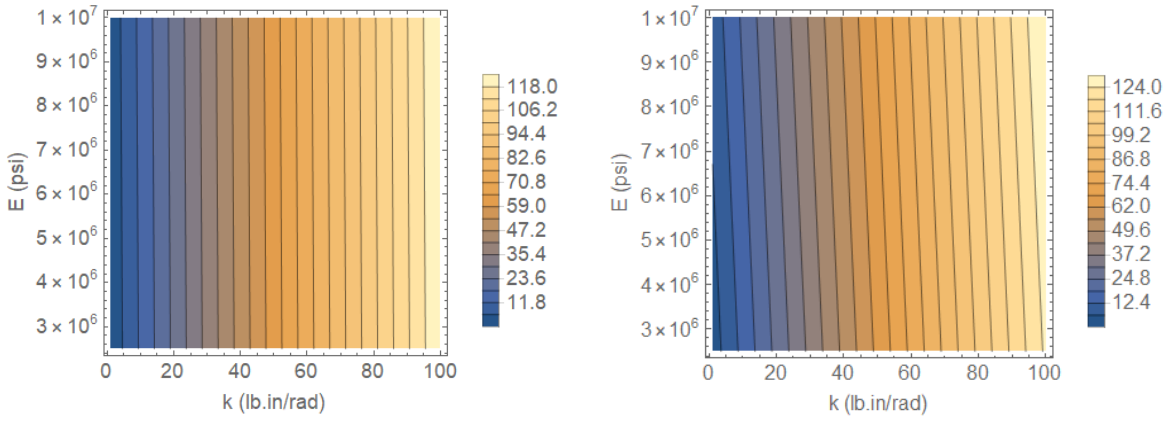

(a) $t = 0.01$ in (b) $t = 0.02$ in

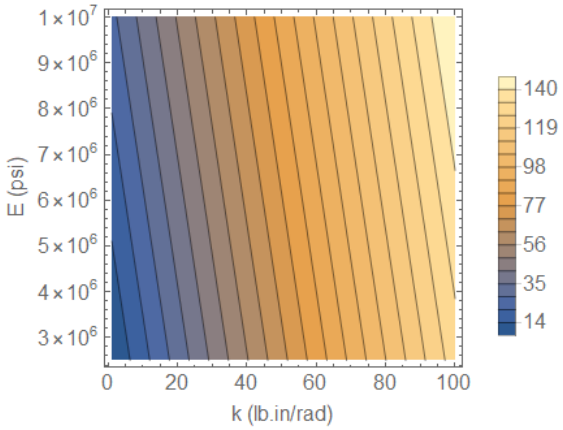

(c) $t = 0.03$ in

Figure 3.2: Elastic energy (lb.in) contour plots for panel elastic modulus and hinge stiffness

to the values of E and t. Elastic energy monotonically increases with the increase in t and E. It can again be inferred that for lower values of t, the value of E doesn't have a large effect. This makes sense since, with larger thicknesses, the factor multiplying E is larger as shown in Eq. 3.5. The large difference in elastic energy values across the contour plots at different hinge stiffness values show the large sensitivity of the elastic energy to k relative to E and t, and Fig. 3.4 confirms that. The influence of t also increases with larger panel elastic modulus, E.

When looking at the graphical results for the fundamental frequency of a uniform panel, it is found that the value of the frequency generally increases with larger values of the design

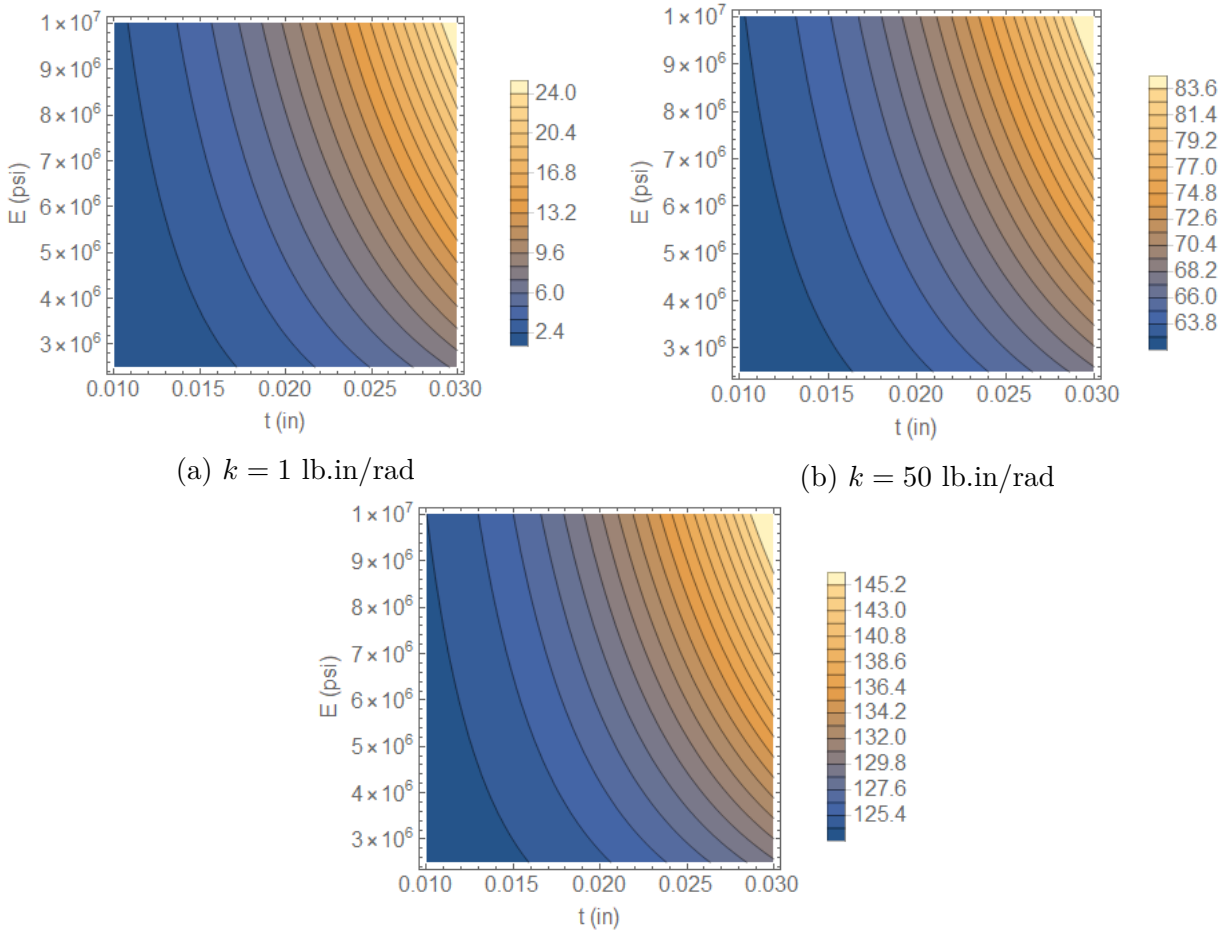

(a) $k = 1$ lb.in/rad

(b) $k = 50$ lb.in/rad

(c) $k = 100$ lb.in/rad

Figure 3.3: Elastic energy (lb.in) contour plots for panel thickness and panel elastic modulus

variables. Figure 3.5 shows that increasing the hinge stiffness past a certain value does not further increase the value of fundamental frequency. For example, for $t = 0.02$ in, a change in hinge stiffness has a significant effect on fundamental frequency up until a hinge stiffness value of around 20 lb.in/rad. That could be attributed to the fact that at large values of k, the hinged panel approaches a cantilever condition.

Figure 3.6 shows that both the thickness and elastic modulus of the panel have very similar influence on the magnitude of the fundamental frequency. That can be inferred since the plots show monotonic increase in fundamental frequency with larger t and E. An exception

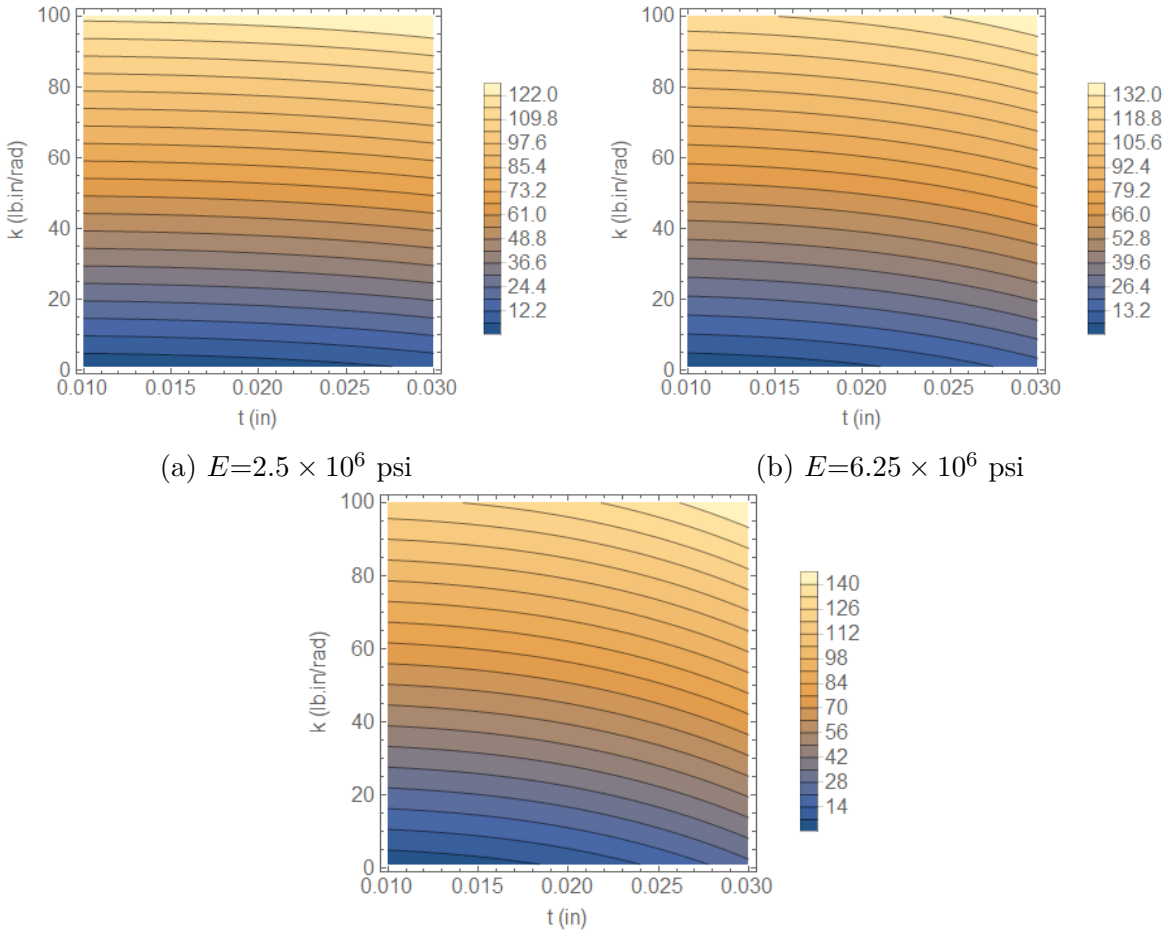

(a) E=2.5 × 10^6 psi

(b) E=6.25 × 10^6 psi

(c) E=1 × 10^7 psi

Figure 3.4: Elastic energy (lb.in) contour plots for panel thickness and hinge stiffness

is seen for a low value of k and a higher value of t shown in Fig. 3.6a. The plot shows that at the lower bound of k, the maximum natural frequency is obtained at a thickness of about 0.025 in and an elastic modulus of 9 × 10^6 psi. This could be due to that at larger thicknesses, the influence of the panel mass on the fundamental frequency takes over that of its stiffness. Fig. 3.7 confirms the conclusion that increasing k past a certain value doesn't further improve the value of fundamental frequency. In the next chapter on results, the optimization will show agreement with the graphical results presented here.

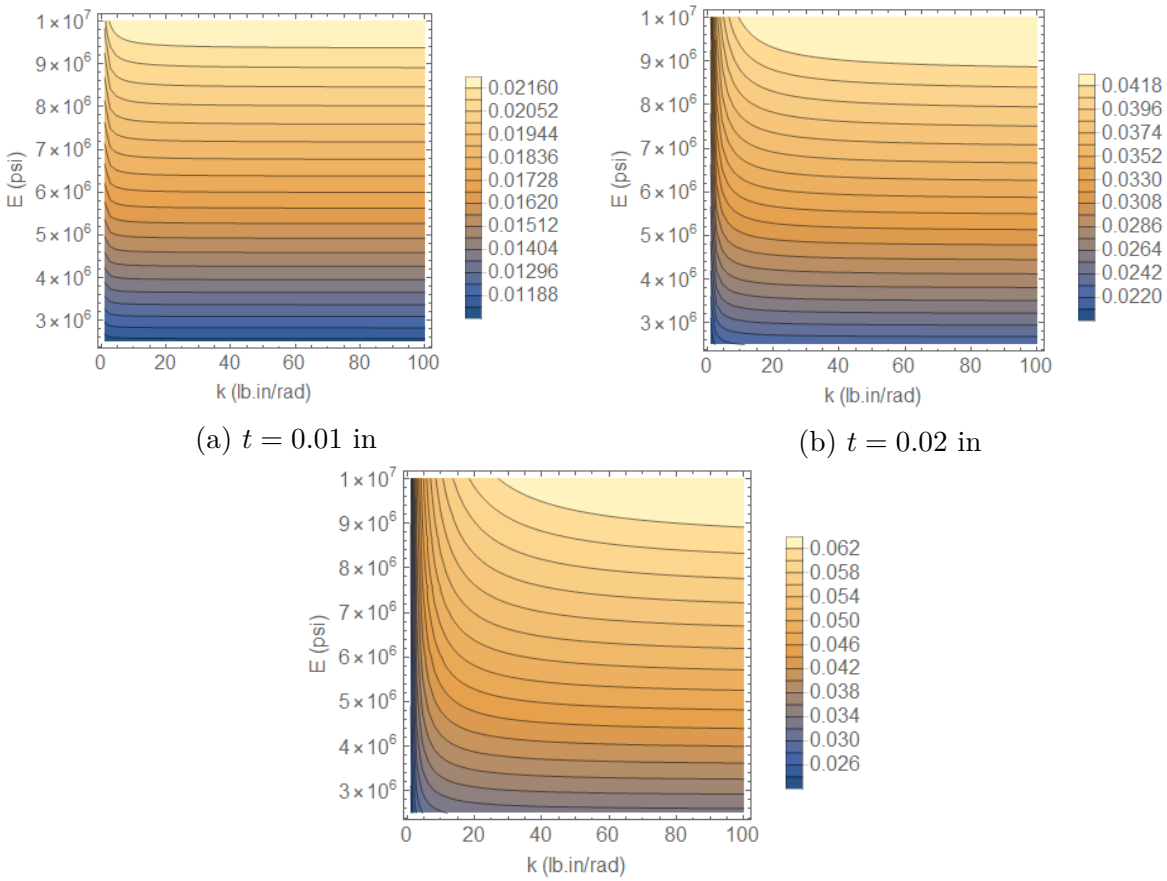

(a) $t = 0.01$ in

(b) $t = 0.02$ in

(c) $t = 0.03$ in

Figure 3.5: Fundamental frequency (Hz) contour plots for hinge stiffness and panel elastic modulus

3.2 Finite Elements Analysis

3.2.1 Energy and Modal Analysis Solutions by FEA

Finite elements analysis (FEA) was used to obtain solutions to the elastic energy and the fundamental frequency of the panel with non-uniform thickness by discretizing the panel into a number of elements. A code for the FEA was developed in Matlab®, and then implemented in Sequential Quadratic Programming and Genetic Algorithm optimizations. For the optimization solved here, the panel was discretized into 40 elements.

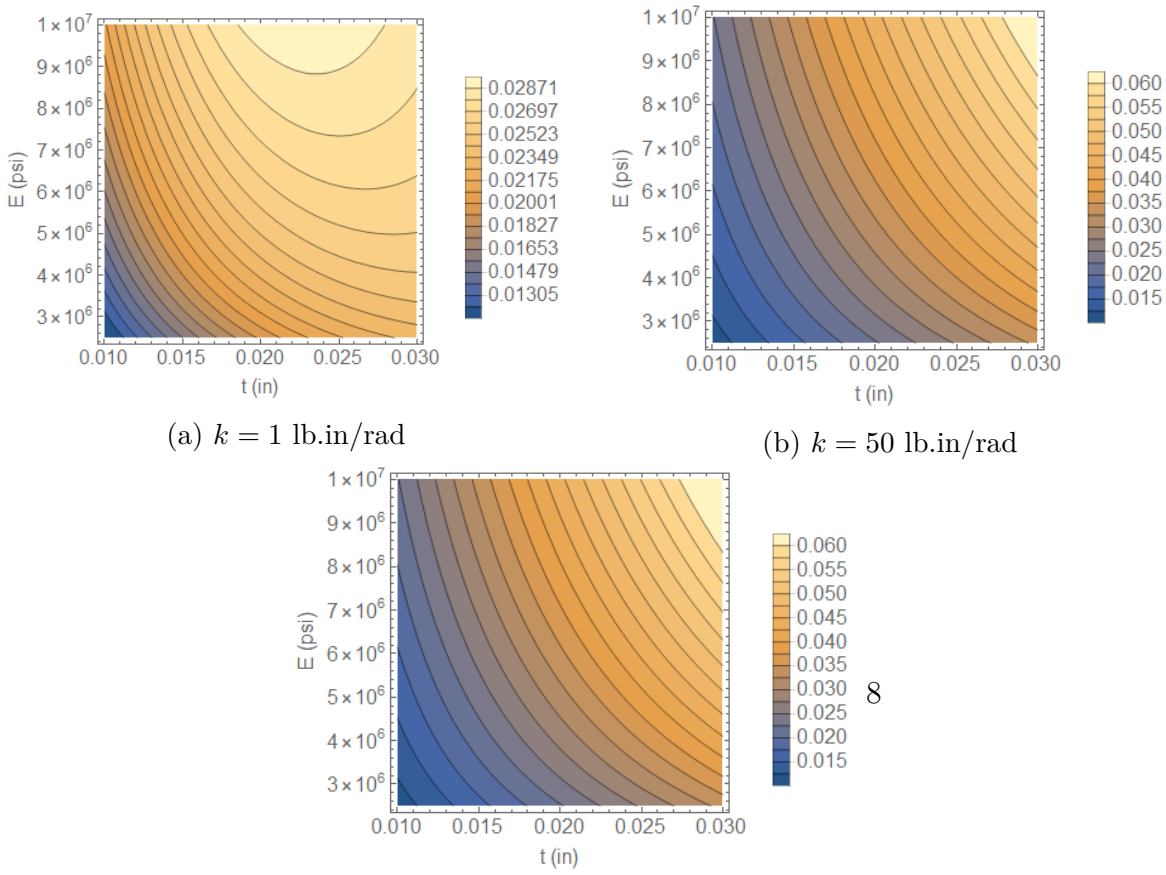

(a) $k = 1$ lb.in/rad

(b) $k = 50$ lb.in/rad

(c) $k = 100$ lb.in/rad

Figure 3.6: Fundamental frequency (Hz) contour plots for panel thickness and panel elastic modulus

The energy objective consists of the sum of each of the panel elements' strain energy added to the potential elastic energy in the rotational spring. Discretizing the panel to n_e number of elements, each allowed to have a different thickness, the strain energy in the panel is given by Eq. 3.16. Thus, the total elastic energy is give by 3.17

$$U_{hinge} = \int_0^L \frac{E\,t^3}{1296}\,dx = \sum_{n=1}^{n_e} \frac{E\,{t_n}^3}{1296}\frac{L}{n_e} \tag{3.16}$$

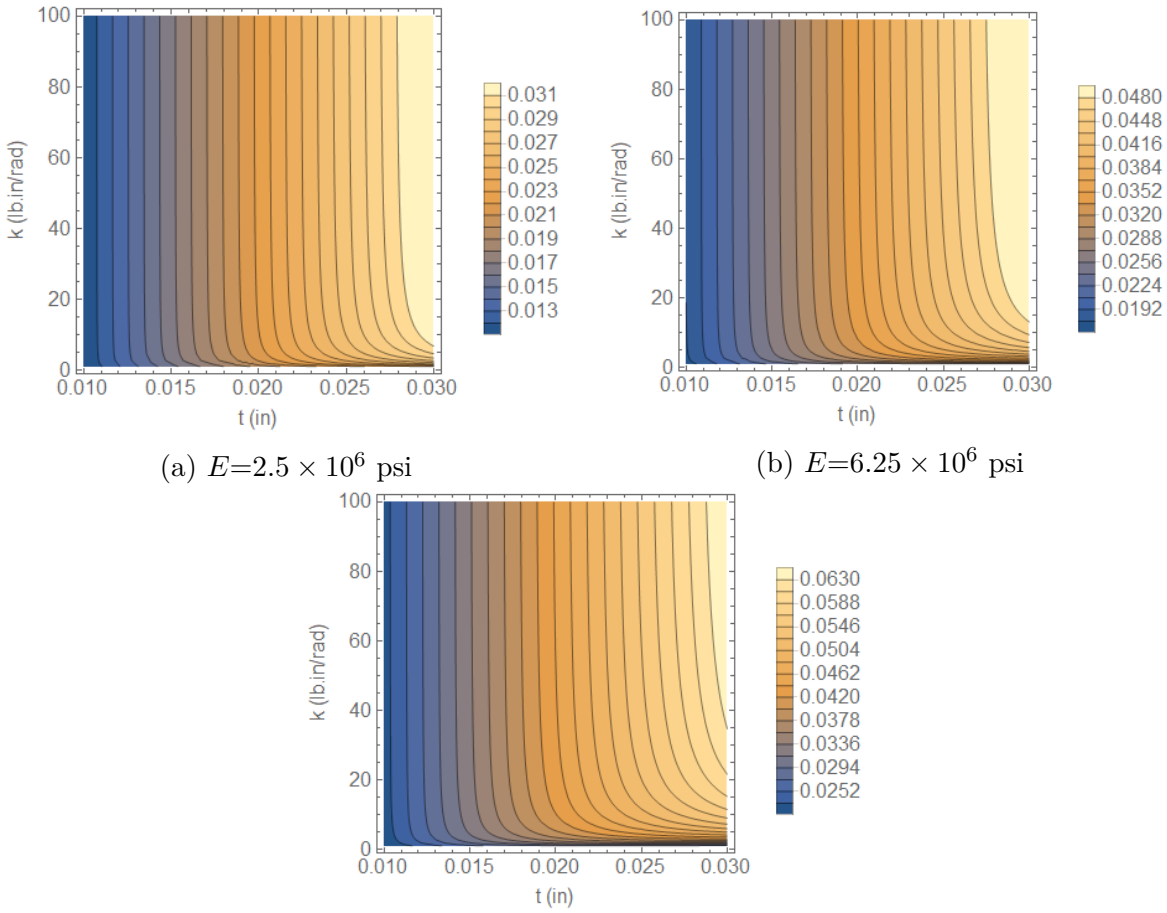

(a) E=2.5 × 10^6 psi

(b) E=6.25 × 10^6 psi

(c) E=1 × 10^7 psi

Figure 3.7: Fundamental frequency (Hz) contour plots for panel thickness and hinge stiffness

$$U = \frac{\pi^2}{8}\, k \; + \sum_{n=1}^{n_e} \frac{E\, {t_n}^3}{1296}\, \frac{L}{n_e} \tag{3.17}$$

For the frequency problem, the stiffness and mass matrices of the beam elements and the linear and rotational springs were assembled, and then the natural frequency was obtained by solving the eigenvalue problem, $([K] - \omega^2[M])\nu = 0$. The first eigenvalue is the square of the fundamental frequency in rad/s. Thus, the square root of the solution was taken and the value was converted to Hz. The stiffness and mass matrix for each panel element are given by 3.18 and 3.19, respectively, where l_e is the length of the element and equals $\frac{120\ in}{n_e}$.

Each element matrix is 4 rows and 4 columns in size, with two degrees of freedom at each node, one corresponding to displacement and reaction force, and the other corresponding to rotation and reaction moment. The global matrices were obtained by assembling the element matrices according to the degree of freedom at the shared nodes. Thus, for the panel consisting of 40 elements, 84 by 84 global mass and stiffness matrices are obtained [19] [3].

$$[K^e] = \frac{2E_eI_e}{le^2}\begin{bmatrix} 6 & 3l_e & -6 & 3l_e \\ 3l_e & 2{l_e}^2 & -3l_e & {l_e}^2 \\ -6 & -3l_e & 6 & -3l_e \\ 3l_e & {l_e}^2 & -3l_e & 2{l_e}^2 \end{bmatrix} \tag{3.18}$$

$$[M^e] = \frac{\rho_e A_e l_e}{420}\begin{bmatrix} 156 & 22l_e & 54 & -13l_e \\ 22l_e & 4{l_e}^2 & 13l_e & -3{l_e}^2 \\ 54 & 13l_e & 156 & -22l_e \\ -13l_e & -3{l_e}^2 & -22l_e & 4{l_e}^2 \end{bmatrix} \tag{3.19}$$

The stiffness matrix for the linear and rotational springs is given by 3.20. Since the end of the springs that is not connected to the panel is fixed, the first 2 rows were eliminated. The global matrix was then assembled such that connectivity of the hinge to the 1st panel node is established.

$$[K_s] = [K_l] + [K_r] = \begin{bmatrix} k_l & 0 & -k_l & 0 \\ 0 & 0 & 0 & 0 \\ -k_l & 0 & k_l & 0 \\ 0 & 0 & 0 & 0 \end{bmatrix} + \begin{bmatrix} 0 & 0 & 0 & 0 \\ 0 & k_\theta & 0 & -k_\theta \\ 0 & 0 & 0 & 0 \\ 0 & -k_\theta & 0 & k_\theta \end{bmatrix} = \begin{bmatrix} k_l & 0 & -k_l & 0 \\ 0 & k_\theta & 0 & -k_\theta \\ -k_l & 0 & k_l & 0 \\ 0 & -k_\theta & 0 & k_\theta \end{bmatrix} \tag{3.20}$$

The Matlab® finite element analysis code can be found in Appendix A. The code was verified by comparing its results for a uniform beam discretized into 40 elements to those obtained by the closed form solutions. The comparison is shown in Table 3.1. The elastic energy FEA solution is exact for a uniform panel since the sum equals the closed form solution.

Table 3.1: Finite element analysis verification

Term	t (in)	E (psi)	k (lb.in/rad)	Close Form Solution	FEA Solution	% Error
U (lb.in)	0.02	5×10^6	10	16.0407	16.0407	0.00
f_n (Hz)				0.03057	0.03056	0.03

3.2.2 Abaqus Modeling and Deployment Simulation

Abaqus® was used to create a simulation for the wrapping and unfurling of the structure. A single panel system identical to the one presented in Fig. 1.1 was created. The panel and hub were connected by a hinge. The hinge was created as a connector of two points at the base of the panel, one of which connects through a coupling constraint to the panel base edge, and the other to the hub surface. The model was assigned values for the design variables, chosen within the constraint bounds, in order to complete and verify the model. The properties of the solid cylindrical hub do not affect analysis results, except for its curvature. Thus, the hub was meshed with 16 quadratic elements, to have a more accurate representation of a smooth circular surface. The flexible panel was meshed by 40 linear elements, and each element was assigned a shell definition to allow for varying thickness.

In order to fully wrap the panel, the hub top and bottom surfaces were constrained to a reference point that rotates to fully wrap the panel. The rotation was defined by a boundary condition on that point, and the rotation angle was calculated based on the circumference and the length of the panel. A second boundary condition was applied to the panel tip to prohibit its movement in the radial direction. This was done so that the panel would

wrap tightly around the rotating hub instead of just rotating with it. For the deployment simulation, the hub was fixed at the fully wrapped orientation, and the panel tip boundary condition was released. Panel wrapping at different time steps of the simulation are shown in Fig. 3.8.

The model was verified by comparing strain energy in the panel obtained by the closed-form solution to that of the simulation at the fully wrapped time step. Modal analysis in Abaqus®was also confirmed to result in a value of fundamental frequency close to that obtained by the closed-form solution. Verification results are presented in Table 3.2.

The energy in both the panel and the hinge is higher than those obtained in the closed form solution. The simulation has a small gap between the panel and the hub to simplify the computation, by avoiding any stresses due to the panel digging into the hub surface. Additionally, the surface of the hub is not perfectly smooth. Due to these reasons, the hinge rotation angle is larger than 90°. The panel elements develop stresses that are not equal throughout the elements. The elements closer to the hinge have high stresses, while the elements at the ends have lower stresses and are wrapped loosely. This discrepancy in the simulation results in higher strain energy than the exact solution; the panel doesn't perfectly follow the curvature of the surface and instead wraps a little tighter. To mitigate some of these error sources in order to make sure the Abaqus® model is a valid representation of the structure, strain energy in the panel was recalculated ignoring the two first and the two last elements. The two elements where the panel connects to the hub and the two at the free end of the panel had stresses that were too high and too low, respectively. The strain energy of the internal elements was divided by 36 to get the average energy in each internal panel element. The average was then multiplied by 40 to get the total strain energy if all panel elements had strain energy equal to the internal elements average. The result in Table 3.2 was improved to 3.99 psi for the strain energy in the panel. Thus, the percent error for

the total elastic in the panel was nearly halved to 7.77%, and the error in total energy of the panel was slightly improved to 8.96%.

Table 3.2: Abaqus strain energy and fundamental frequency results verification

Term	t (in)	E (psi)	k (lb.in/rad)	Closed Form Solution	Abaqus Solution	% Error
U_{panel}(lb.in)	0.02	5×10^6	10	3.704	4.294	15.93
U_{hinge} (lb.in)				12.337	13.486	9.31
U(lb.in)				16.0407	17.780	10.84
f_n(Hz)				0.03057	0.03057	0.00

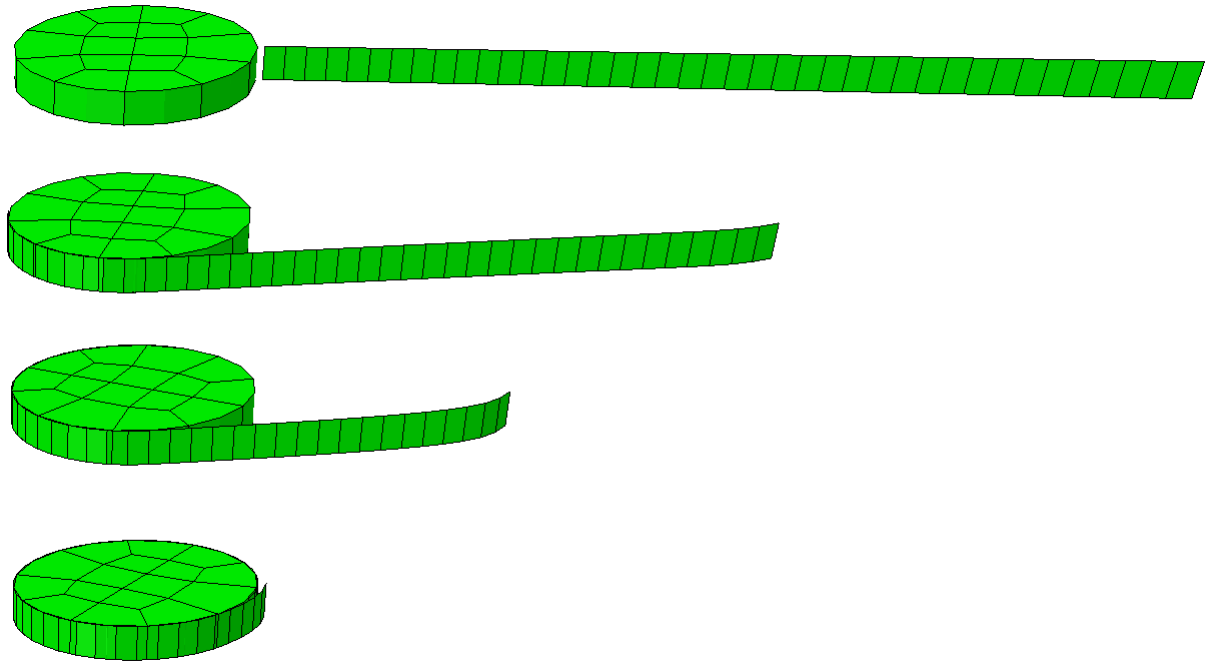

Figure 3.8: Wrapping simulation by Abaqus®

Material damping definition was added to the panel, to realistically model the behavior of the deployment simulation. The damping was defined through the specification of mass and stiffness proportional damping coefficients, α and β, in Abaqus®. The coefficients were calculated based on two natural frequency values of the panel and for a given critical damping ratio that is equal for both frequencies, as shown in Eq. 3.21 and Eq.3.22 [26]. Continuous

metal structures have critical damping ratios between 2% and 4% [1], so, a value of 3% was specified for our panel. The mass and stiffness proportional damping was calculated for the first and second natural frequencies of the panel, which in turn depends on values of the design variables. Thus, for the equations below, $i = 1$ and $j = 2$.

Mass proportional damping coefficient:

$$\alpha = 2\,\xi \frac{\omega_i\,\omega_j}{\omega_i + \omega_j} \tag{3.21}$$

Stiffness proportional damping coefficient:

$$\beta = \frac{2\,\xi}{\omega_i + \omega_j} \tag{3.22}$$

After the single panel simulation was successful, three symmetric panels were added at a 90° angle from each other around the hub. The hub was connected to a spacecraft modeled as a solid cuboid. The panels were wrapped around the hub, and then the deployment simulation was run for a free-free system. The objective of the multi-panel deployment simulation was to observe the deployment behavior with regards to the stiffness of the panels and the energy released as they unfurl in a system that more accurately resembles possible applications. Thus, the deployable structure was connected to a spacecraft of realistic mass and inertia values. Specifically, the spacecraft was assumed to have a mass of 27 slugs and an inertia about the z-axis equal to 4,000 slugs.in^2. The inertia was implemented in the model through specifying the dimensions of the cuboid and was based on inertia values of a reference spacecraft with the mass specified. The mass was applied to the model through the selection of the cuboid material density. The height of the cuboid in the model is about 52 in while the width and depth are 36 in and 22 in, respectively. The Abaqus® model is shown in Fig. 3.9.

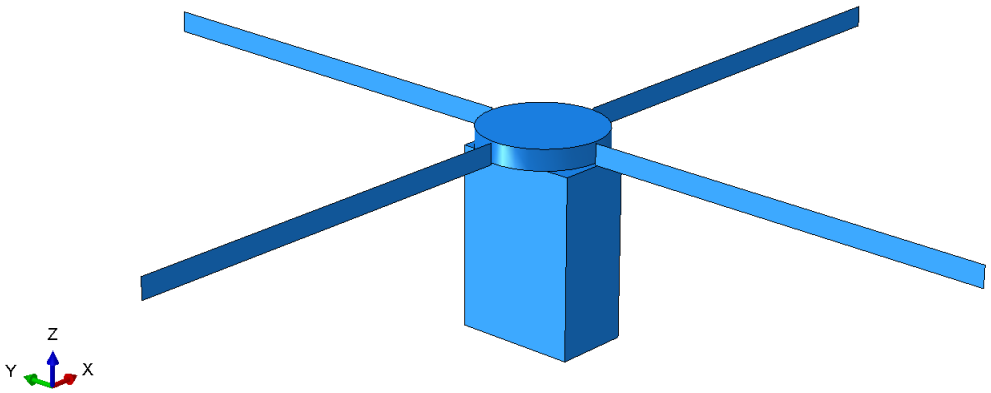

Figure 3.9: Abaqus® deployable structure and spacecraft model

The hub was connected to the spacecraft simulator by a stiff hinge. The stiffness value of the connector was set to 1×10^5 lb.in/rad. In order to assess the behavior due to the deployment of the panel alone, the hub and spacecraft were rotated together in the wrapping simulation, so that no energy is stored in the hinge connecting them. Damping in spacecraft is present due to structural damping and damping of its components and joints. The damping ratio of spacecraft generally fall between 2 and 10% [25]. Damping was added to the hinge to represent a damping ratio of the higher value of 10%, which can reflect damping integrated in the hinge design in addition to the spacecraft damping for possible applications. The damping coefficient of the hinge was calculated based on the damping ratio. Given that the spacecraft and hinge are a simple rotational spring-mass-damper system, the critical damping can be calculated as shown in Eq. 3.23 [2], where I is the spacecraft inertia, and k_r is the stiffness of the hinge. The damping coefficient was calculated by Eq. 3.24.

$$C_c = 2\sqrt{k_r I} \tag{3.23}$$

$$\xi = \frac{C}{C_{cr}} \tag{3.24}$$

The results were assessed to ensure that the optimization formulation is appropriate and gives desired results. The four-panel deployment simulation was run for parameter values resulting from the genetic algorithm optimization by Isight® discussed in the following section. The genetic algorithm was run multiple times for different objective function formulations, and the results implemented in the model were those of the run resulting in the highest strain energy. This was done to verify that the spacecraft remains stable and there is no violent rotation due to the unfurling panels. The deployment simulation animation was observed, and the rotation angle at a node on the spacecraft was output. Additionally, the stress in the panel elements for all time steps was returned to confirm it remains well below the constraint value. The simulation was run for three minutes from the release of panel.

3.3 Methods and Tools of Optimization

The finite element analysis code developed in Matlab® was used to solve the optimization problem, discussed in Section 1.2. Two optimization methods were used: Sequential Quadratic Programming and Archive based Micro Genetic Algorithm.

Mathworks Matlab® built in function, fmincon, was run with Sequential Quadratic Programming (SQP) option. Fmincon is a nonlinear optimization that finds the minimum of a constrained multivariable function [13]. SQP is a trust region method, where the function to be minimized is approximated by a simpler function that resembles its behavior in a neighborhood around a point, x [12]. This neighborhood is known as the trust region, and a trial step is conducted by minimizing over that region. Iterations proceed as the function value is improved. When the solver reaches an iteration where the function value is not minimized, the trust region size is reduced. In SQP, the Hessian of the Lagrangian function is approximated at every major iteration by a quasi-Newton method. The Hessian approximation is

then used to create a quadratic subproblem that is solved to specify the search direction. Additionally, any nonlinear constraints are linearized in the subproblem. A new iteration is then conducted, based on a step size that sufficiently decreases the function. This is repeated until the solver converges to a solution.

Archive based Micro Genetic Algorithm (AMGA) optimization was run by a commercially available Multi-Disciplinary Optimization (MDO) tool, Simulia Isight®. Isight® allows the combination and automated execution of multiple applications and processes in a simulation process flow [7]. The FEA Matlab® code discussed in Subsection 3.2.1 that calculates the objective and constraint values was executed in the simulation flow, specifying input variables and their initial values, as well as output variables to be solved for in the optimization. An optimization component follows Matlab in the simulation flow, and allows the specification of design variables, constraints, and objectives. The simulation flow is shown in Fig. 3.10.

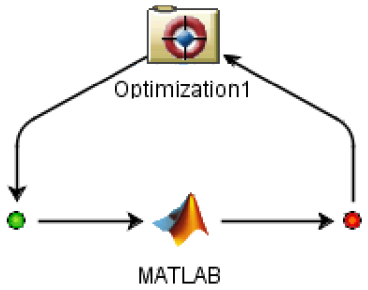

Figure 3.10: Simulia Isight® simulation flow for the optimization of the unfurlable structure

AMGA was selected from a number of multi-objective optimization methods available in Isight®. The optimization method selection window in Isight® describess AMGA as a non-gradient based method well suited for highly nonlinear search spaces. The methods treats each objective function separately and builds a pareto front by choosing feasible non-dominated designs. AMGA was developed by Tiwari, Koch, Fadel, and Deb [22]. It is an evolutionary optimization algorithm that, since new solutions are obtained through genetic

variation operators and the solutions created before a given iteration is used in the selection process. Every iteration of AMGA produces a small number of solutions that are used to update the archive, and the search history is utilized to reduce the required number of function evaluations. The optimization problem was defined identically as in the SQP optimization, and results were compared. Additionally, AMGA was run for a few different weights and formulations of the objective function, as discussed in Section1.2. Results are presented and discussed in the following chapter.

Chapter 4

Results and Discussion

4.1 Optimization Results

4.1.1 SQP Results

Fmincon was run for a single objective function consisting of the fundamental frequency function, f_n, multiplied by a weight of $10,000$ and subtracted from the elastic energy function,U, as shown in Eq. 4.1. The convergence and results of SQP can be highly affected by initial values of the design variables. To obtain the best results, the algorithm was run 100 times for randomly generated initial points of the design variables within the constraint bounds. The lowest resulting objective value of the runs was returned. Figure 4.1 shows the thickness results for the panel elements, where element 1 corresponds to the base of the panel that connects to the hinge, and element 40 is the last element at the free end. Table 4.1 lists the results for the design variables, each objective function term, and the total objective.

$$f_{objective}(E, k, t) = U - 10,000 \times \ f_n \tag{4.1}$$

Table 4.1: SQP optimization results

k (lb.in/rad)	E (psi)	U (lb.in)	f_n (Hz)	$f_{objective}$
25.11	9.35 E6	40.67	0.039	-352.68

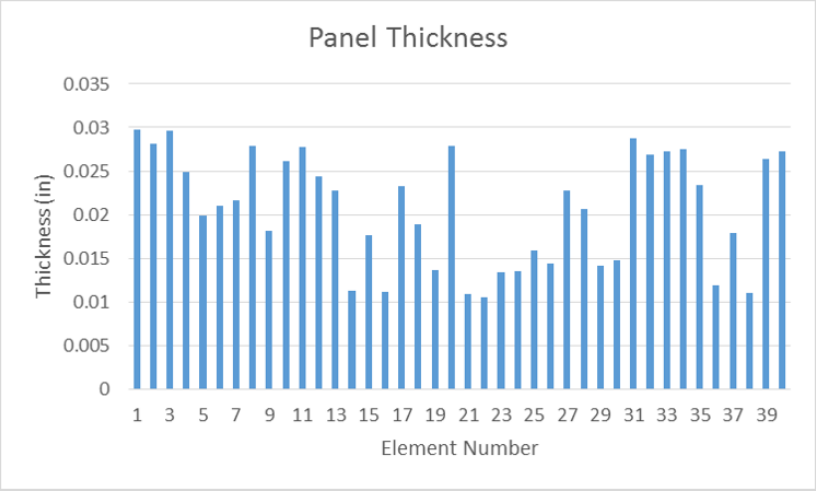

Figure 4.1: SQP optimization panel thickness results

The weight that multiplies the fundamental frequency function was based on the order of magnitude of elastic energy and fundamental frequency given the design variable bounds. The possible values of elastic energy are on the order of magnitude from 1 and 100. On the other hand, the fundamental frequency values are on the order of magnitude of 0.01. For this formulation, the weight of 10,000 given to the fundamental frequency gives it high importance, as is apparent in the elastic modulus value. Additionally, the hinge stiffness value of 25.11 lb.in/rad agrees with the graphical results presented in Section 3.1.2. It was concluded from the contours that increasing the stiffness past a value of around 20 lb.in/rad doesn't further increase the frequency value. Although the stiffness and modulus of elasticity show expected results, the panel elements thickness results indicate that SQP does not converge to a global minimum. That is because the thicknesses don't follow any specific trend and seem random. Additionally, the results are not repeated when SQP is run again. Thus, although SQP converged to a solution, that solution did not correspond to a global optimum, but rather, different local optima depending on the initial variables value. For some of the starting points, SQP failed to converge to a minimum. This was attributed to the fact that the objective function terms are highly non-linear and would be more suited

for a non-gradient based optimization.

4.1.2 AMGA Results

First, AMGA was run in Isight® for the same fundamental frequency function weight as that in SQP, given in Eq.4.1. AMGA results are given in Table 4.2 and Fig. 4.2. It can be seen that the thickness of beam follows a tapered shape, as expected with the high influence of fundamental frequency on the objective outcome due to the large weight multiplying the frequency objective term. These results further confirm the conclusion that SQP did not converge to the global optimum. Conversely, the hinge stiffness and panel elastic modulus values agree with those of SQP fundamental frequency, where E is at its upper bound, and k is close to the value that yields maximum fundamental frequency. Comparing the results of the two methods, it was found that fundamental frequency was improved by 136%. Given the weight of the fundamental frequency term, the overall objective, $f_{objective}$ was decreased by around 142%, despite the fact that the elastic energy is 54% higher in the AMGA results.

Table 4.2: AMGA optimization results for fundamental frequency function weight of 10,000

k (lb.in/rad)	E (psi)	U (lb.in)	f_n (Hz)	$f_{objective}$
38.92	1.00E7	62.74	0.092	-852.73

Next, AMGA was run for a lower weight for the fundamental frequency term. The fundamental frequency objective term was multiplied by 1,000, and as expected, the thickness didn't follow the taped shape as smoothly as with the higher weight value, as shown in Fig. 4.3. Result for this run are shown in Table 4.3. The elastic modulus is also near the upper bound for this run, while the hinge stiffness is lower. Although the obtained fundamental frequency is lower than the proceeding run, the elastic energy is also lower as desired in the optimization. Higher weight values mean larger influence of the multiplied term on the opti-

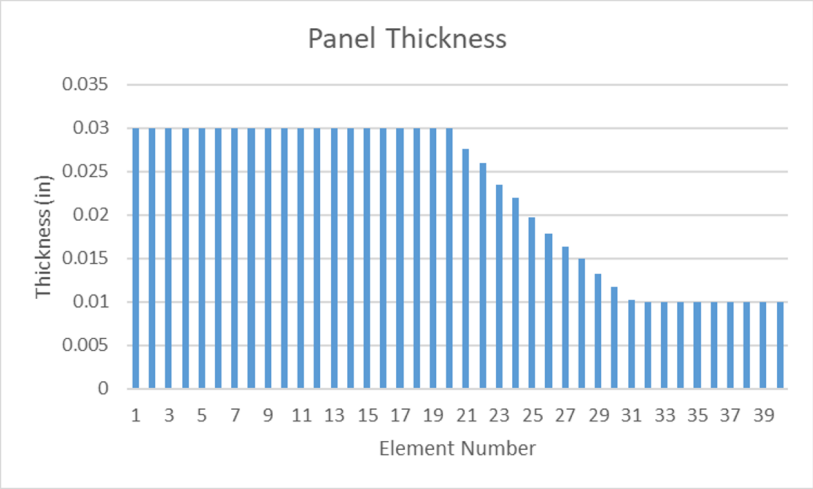

Figure 4.2: AMGA optimization panel thickness results for fundamental frequency function weight of 10,000

mization results, which translating into better results for that objective. Since our objective function terms are contradicting with respect to the design variables, an improvement in one of the terms results in a trade off in the other.

Table 4.3: AMGA optimization results for fundamental frequency function weight of 1,000

k (lb.in/rad)	E (psi)	U (lb.in)	f_n (Hz)	$f_{objective}$
9.32	9.997 E6	24.40	0.079	-54.31

Following that, the same formulation with the weight of 1,000 was run with an added mass constraint, given by Eq. 1.9 in Section 1.2. The resulting thicknesses, shown in Fig. 4.4, follows the tapered shape even less when the mass is constrained to 70% of the maximum possible value given the upper bound of thickness. Adding the mass constraint also resulted in higher energy and lower frequency, opposite to the desired results from the optimization, as presented in Table 4.4. Thus, the other runs were made without including a mass constraint.

Two more optimizations were performed. First, an even lower weight of 100 was multiplied by the fundamental frequency objective. As expected from previous results, the lower weight resulted in thicknesses that are more random, and do not follow a tapered shape well.

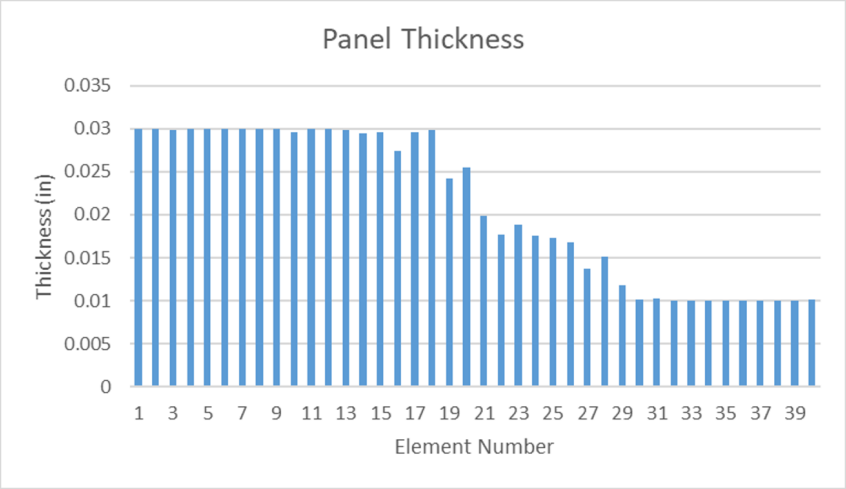

Figure 4.3: AMGA optimization panel thickness results for fundamental frequency function weight of 1,000

Table 4.4: AMGA optimization results for fundamental frequency function weight of 1,000 with mass constraint

k (lb.in/rad)	E (psi)	U (lb.in)	f_n (Hz)	$f_{objective}$
3.23	9.96 E6	26.32	0.061	-34.77

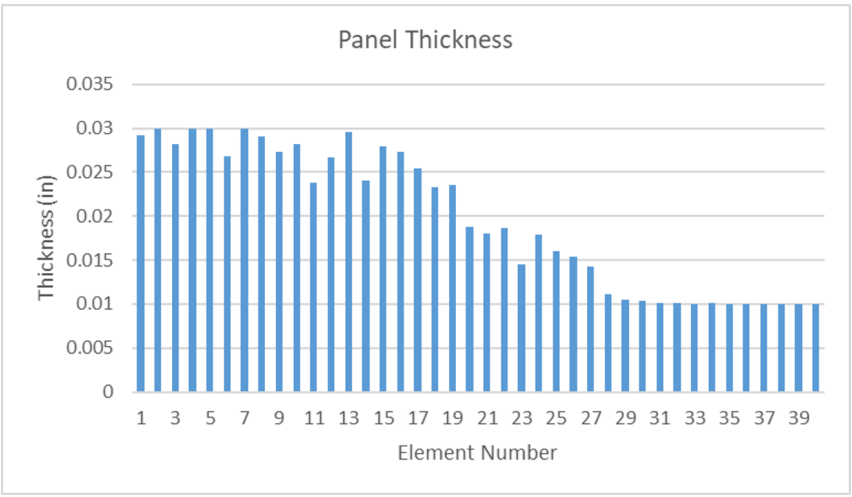

Figure 4.4: AMGA optimization panel thickness results for fundamental frequency function weight of 1,000 with mass constraint

Additionally, the fundamental frequency value is lower and so is the elastic energy. Thus, we can conclude that changing the weight can be used to achieve certain frequency of energy

requirements. The elastic modulus for this run in near the lower bound, conversely to the previously presented runs. The hinge stiffness for this run is also at the lower bound. Results for this optimization are given in Table 4.5 and Fig. 4.5.

Table 4.5: AMGA optimization results for fundamental frequency function weight of 100

k (lb.in/rad)	E (psi)	U (lb.in)	f_n (Hz)	$f_{objective}$
1.00	2.51 E6	2.30	0.024	-0.098

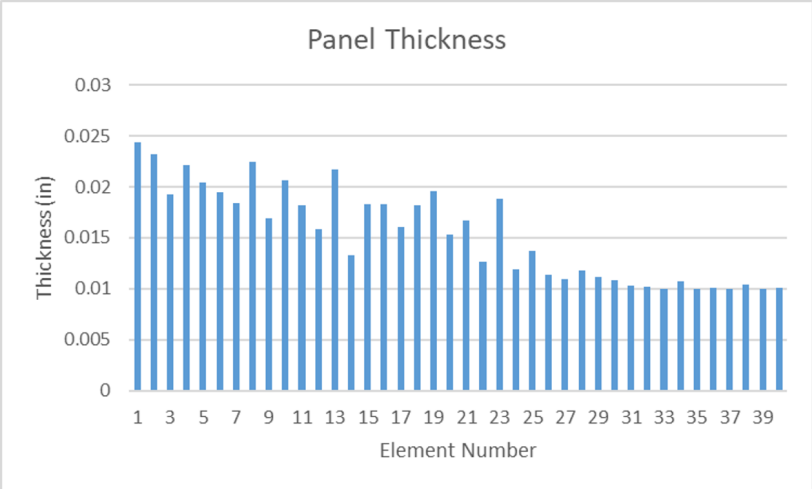

Figure 4.5: AMGA optimization panel thickness results for fundamental frequency function weight of 100

The last run was using the reciprocal of the fundamental frequency as the objective function term to be minimized, rather than minimizing the negative of the fundamental frequency value. The formulation presented in Eq. 4.2 results in the lowest elastic energy value, as shown in Table 4.6. This formulation shows a good trade off in two objective function values and is comparable to the other runs. The thickness results for this run are given in Fig. 4.6, and show that the shape of the panel is not a very smooth tapered beam. Depending on the specific application, the weights and formulations presented here can be selected to achieve desired results. It is worth mentioning that the machining of a tapered panel would be less challenging than that of a more random thickness.

$$f_{objective}(E, k, t) = U + \frac{1}{f_n} \tag{4.2}$$

Table 4.6: AMGA optimization results for the elastic energy added to the reciprocal of fundamental frequency

k (lb.in/rad)	E (psi)	U (lb.in)	f_n (Hz)	$f_{objective}$
3.16	7.83 E6	9.54	0.051	29.03

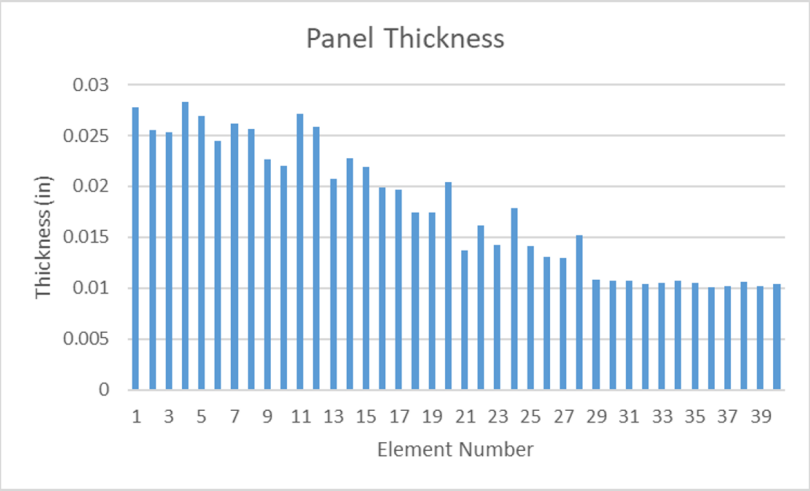

Figure 4.6: AMGA optimization panel thickness results for the elastic energy added to the reciprocal of fundamental frequency

4.2 Deployment Simulation Results

The deployment simulation was run for the results of AMGA that gave in the highest elastic energy, namely the run where the fundamental frequency was multiplied by 10,000. These values were chosen to confirm that the optimization results and formulation produce desirable deployment behavior, where the panel fully deploys without inducing excessive rotation in the spacecraft even at the highest obtained elastic energy values.

The three minute deployment simulation showed that the panel fully deploys in 1.3 seconds. The panel then goes beyond the fully wrapped position, and, with its momentum, contact the hub again in the other direction and nearly fully wraps again. Oscillations continue around the hinge with some wrapping for a number of times, until the motion damps out. The oscillations are almost completely damped out by the end of the three minutes, with a small amplitude of oscillation remaining. Figure 4.7 (a) through (j) shows the deployment simulation at multiple time steps. The rotation in the connected spacecraft, which is unconstrained to represent on-orbit free-free boundary conditions, is shown in Fig. 4.8. The rotations plot generated in Abaqus®shows small angles of oscillation in the spacecraft. At the end of the three minutes, the spacecraft rotated a total of 1 rad, or around 60°, from the position at the beginning of the unfurling simulation. Figure 4.9 shows the total elastic energy in both the panel and hinge during the three minutes of the simulation. The elastic energy reflects the panel's oscillating motion, wrapping and unfurling in either direction a few times, while the energy is being being damped out with increasing time until the motion is completely damped out and the elastic energy is zero. Finally, the maximum stresses in the panel elements were found to be around 55 ksi, which is well below the allowable maximum of 250 ksi. The von Mises stress in each element for each time step are shown in Fig. 4.10. It can be concluded that the optimization formulation is appropriate in terms of the studied objectives since the panel unfurls efficiently and does not cause unstable motion in the spacecraft.

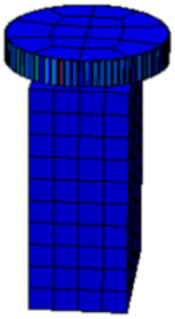

(a) The panel is fully wrapped at *t=0* s

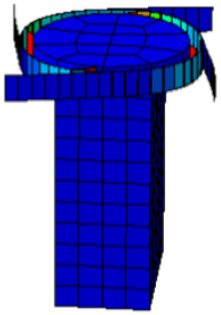

(b) Deployment Begins (*t=0.08* s)

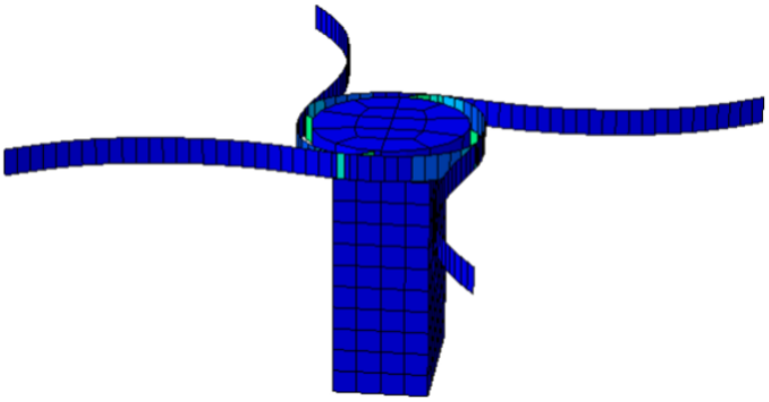

(c) (*t=0.36* s)

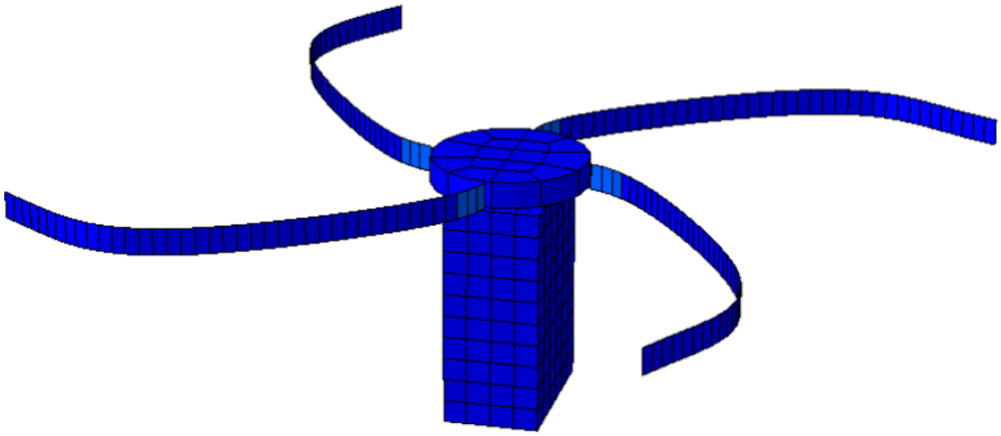

(d) (*t=1.03* s)

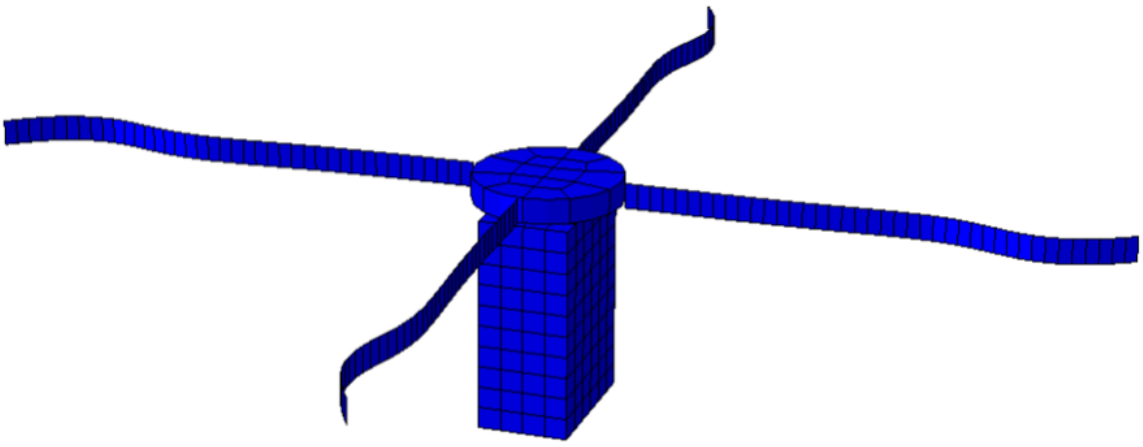

(e) The panel reaches the fully deployed position at *t=1.3* s

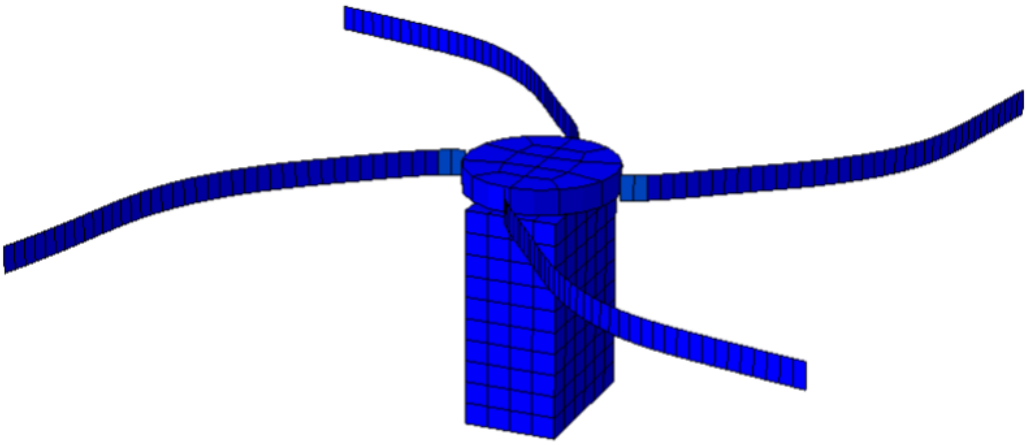

(f) The panel continues beyond the fully deployed position and start wrapping around the hub in the other direction (*t=1.6* s)

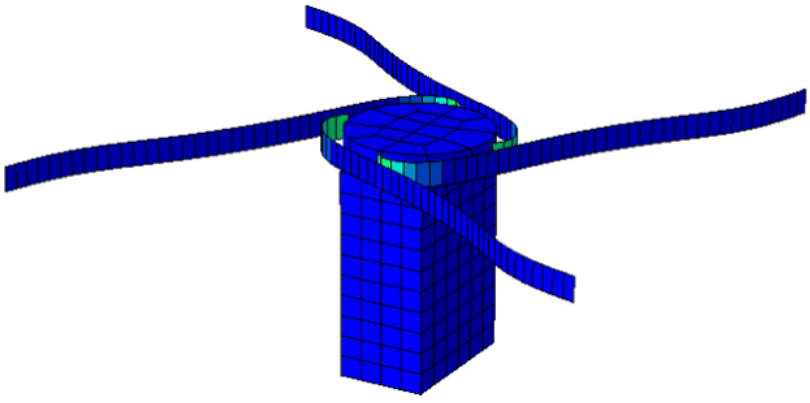

(g) (*t=2.2* s)

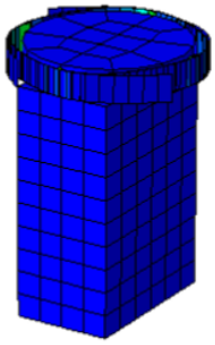

(h) The panel wraps loosely around the hub on the other side at *t=2.8* s

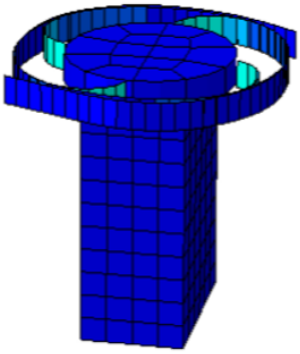

(i) The panel continues to oscillate, wrapping around the hub on either side. The wrap continues to get looser as energy is damped (*t=6.6* s)

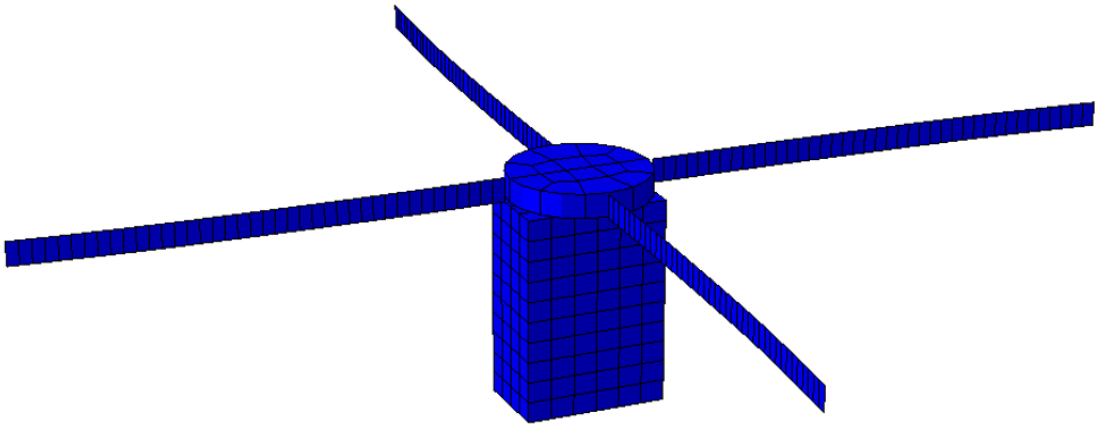

(j) Motion damps out and the panel is in the fully deployed configuration at *t=180* s

Figure 4.7: Unfurlable structure deployment simulation in Abaqus® at multiple time steps

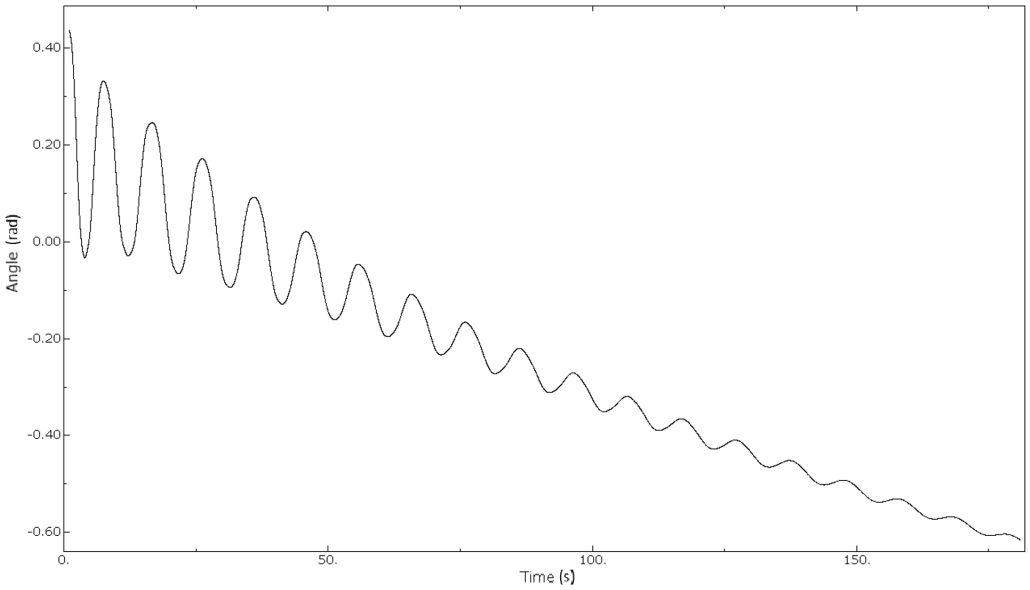

Figure 4.8: Rotation angle of a node on the spacecraft for the duration of the deployment simulation

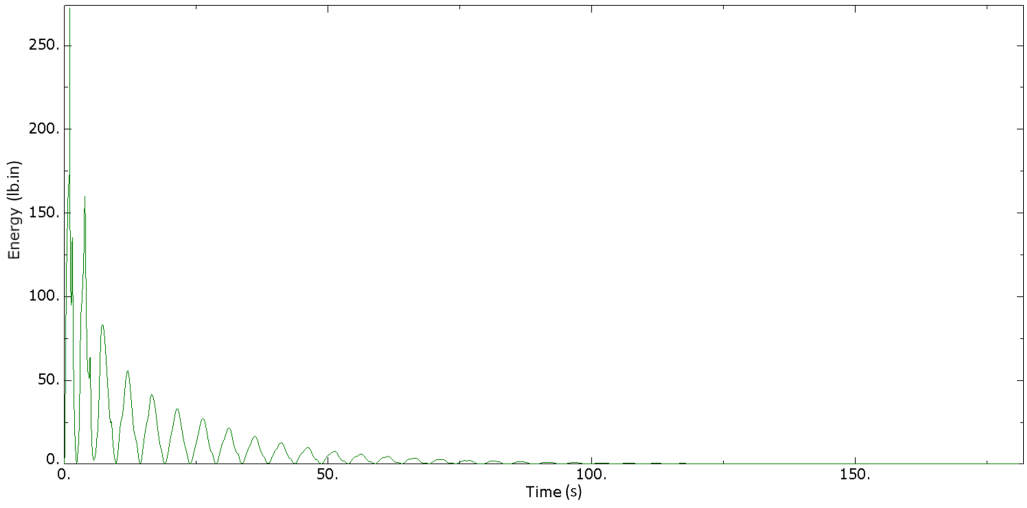

Figure 4.9: Total elastic energy in the panel elements and the hinge for the duration of the deployment simulation

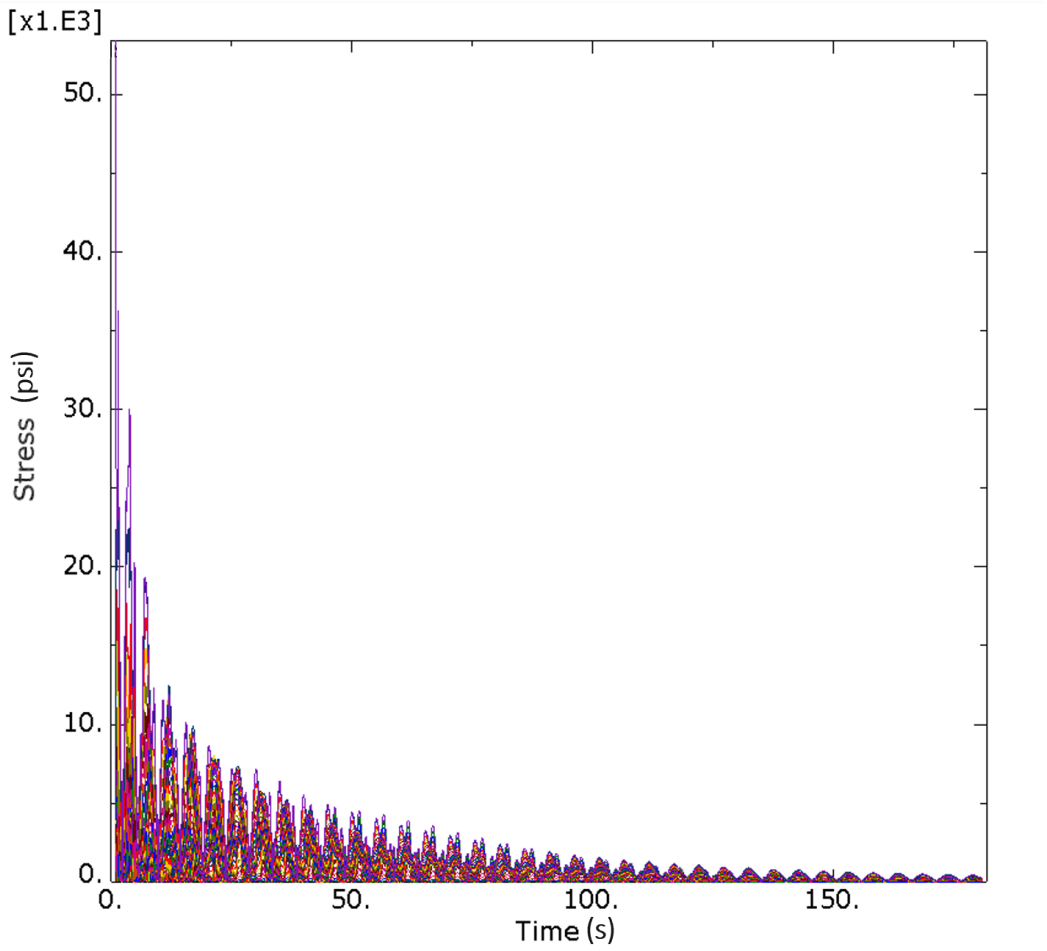

Figure 4.10: Von Mises stress in each element of the panel for the duration of the deployment simulation

Chapter 5

Summary, Conclusions and Future Work

In this research, a generic unfurlable structure consisting of a thin hinged rectangular panel that wraps around a central cylindrical hub was optimized. The goal of the study was to better understand the underlying analysis and behavior of this type of deployable structures, and develop a approach by which to optimization such structures. The specified objectives were to maximize the fundamental frequency of the deployed panel and minimize the stored elastic energy in stowed hinge and panel. These objectives were achieved by finding the optimum values of the stiffness of the hinge, the elastic modulus of the panel and the thickness of the panel. The results of the optimization were implemented in a dynamic deployment simulation, to assess the behavior and verify the effectiveness of the developed optimization formulation.

The closed form solutions were obtained for the two objectives assuming a uniform panel, and their contours were plotted to better understand the dependency of each of the objective function terms on the three design variables. The two objectives are contradicting since they are both directly proportional to the design variables. The elastic energy was found to highly depend on the value of k compared to that of t. This can be understood since the allowed thickness values are on the order of 0.01 in, and thickness is cubed in the elastic energy equation. The elastic modulus of the panel, E, also has a small effect on the elastic energy

compared to the effect of k. The influence of t increases with larger values of E, and vice versa. The fundamental frequency is influenced to a relatively similar extent by variations in E and t. The increase is monotonic except high thickness values for lower k values. In that case, the effect of the mass of the panel on the frequency overtakes that of the stiffness. The value of k has a substantial effect on the fundamental frequency up to a certain value between around 10 and 40 lb.in/rad based on the thickness, after which an increase in k does not result in any further increase in frequency.

Solutions to the objective functions were defined by finite element analysis, which was used in the optimization. Two methods of optimization were performed, SQP and AMGA, and the panel was allowed to have varying thickness for each of its elements. Different weights were given to the fundamental frequency objective, so that the order of magnitude is comparable to that of the elastic energy. This was done since the objective for both SQP and AMGA is computed as a sum of the elastic energy and the negative of the fundamental frequency, since the overall objective is to be minimized. SQP was only run for the highest specified weight, and it was found that it does not converge to a global minimum, but rather, a local minimum based on the specified initial values of the design variables. This was concluded since the resulting thickness of the panel elements did not follow a tapered shape as expected. AMGA resulted in a tapered panel for the run of identical weight and formulation. As the weigh of the fundamental frequency objective was decreased, the panel's thickness less closely followed a tapered beam, and became more random. A different formulation where the maximization of the fundamental frequency was implemented by minimizing the reciprocal was also performed. The results were comparable to those of the simple sum formulation, but the resulting elastic energy was the lowest of the runs. The optimization results agreed with those found in the graphical solutions, where the stiffness did not exceed 40 lb.in/rad, even for higher fundamental frequency weights. The weights can be selected based on which

objective deemed to be of higher importance based on the application.

The panel was modeled in Abaqus® to observe the deployment behavior of the optimized panel and hinge. A one panel model was created to achieve successful wrapping and to verify the model against the closed form solution. After this was completed, additional panels were added to the model for a total of four panels at 90 degrees from each other around the hub. The hub was also attached to a solid cuboid representing a spacecraft's mass and inertia. The hinge connecting the spacecraft to the hub was highly stiff, and was assigned a damping coefficient value corresponding to a critical damping ration of 10° for the spacecraft. The deployment was run for a free-free deployable structure and spacecraft system, and it was found that the deployment is efficient, where the panel reaches the fully deployed configuration in about 1.3 seconds, after which it continues to largely oscillate until the motion is nearly fully damped after 3 minutes. Small rotation is induced in the connected spacecraft, which only rotates by about 60° from its starting position as the panel unfurls.

In future work, the deployment behavior can be further studied and possibly optimized. Large oscillations are not desirable in many applications, and accurate deployed shape is critical to some missions. Thus, formulating an optimization problem of parameters related to the deployment of the panel and its final shape would be a desired in future work. Additionally, supporting flexible components representing wires or meshes could be modeled between the panel to better represent possible applications. The behavior of these element needs to be better understood to be accurately modeled. Other components can be also added to the deployable structure to get better deployment results. This study was done for a simple and generic structure, and its results can be used and expanded on for the optimization and analysis of more complex deployables in the future.

Bibliography

[1] Vince Adams and Abraham Askenazi. *Building better products with finite element analysis*. Cengage Learning, 1999.

[2] Ralph E Blake. Basic vibration theory. *Shock and vibration handbook*, 1:2–8, 1961.

[3] Malkus D. S. Plesha M. E. Cook, R. D. and R. J Witt. *Concepts and Applications of Finite Element Analysis*. Wiley, New York, 4th edition, 2002.

[4] João Fernandes da Silva, Lucas Allende Dias do Nascimento, and Simone dos Santos Hoefel. Free vibration analysis of euler-bernoulli beams under non-classical boundary conditions. 2015.

[5] Andrea E Del Grosso and Paolo Basso. Deployable structures. In *Advances in Science and Technology*, volume 83, pages 122–131. Trans Tech Publ, 2013.

[6] BS Gaudi, S Seager, B Mennesson, and A Kiessling. Habex: The habitable exoplanet observatory interim report, 2018.

[7] Simulia Isight. Isight: Automate design exploration and optimization, 2014. URL https://www.3ds.com/fileadmin/PRODUCTS-SERVICES/SIMULIA/RESOURCES/simulia-isight-brochure.pdf.

[8] P. Kelly. *Solid Mechanics Lecture Notes*. 2013. URL http://homepages.engineering.auckland.ac.nz/~pkel015/SolidMechanicsBooks/Part_I/index.html.

[9] Gokhan Kiper and Eres Soylemez. Deployable space structures. In *2009 4th International Conference on Recent Advances in Space Technologies*, pages 131–138. IEEE. ISBN 1424436265.

[10] Do Hyuk Kwak, Hwa Young Jung, Jae Eun Lee, and Kwang Hee Kang. Material analysis and shape optimization of a deployable lightweight satellite antenna reflector. *Journal of The Korean Society of Manufacturing Technology Engineers*, 26(2):185–192, 2017. ISSN 2508-5093.

[11] Mark S Lake, Lee D Peterson, Martin M Mikulas, Jason D Hinkle, Lisa R Hardaway, and Johanne Heald. Structural concepts and mechanics issues for ultra-large optical systems. In *1999 Ultra Lightweight Space Optics Workshop*.

[12] Mathworks. Constrained nonlinear optimization algorithms, . URL https://www.mathworks.com/help/optim/ug/constrained-nonlinear-optimization-algorithms.html.

[13] Mathworks. fmincon, . URL https://www.mathworks.com/help/optim/ug/fmincon.html.

[14] Leonard Meirovitch. *Fundamentals of Vibrations*. Waveland Press, 2010.

[15] Mehran Mobrem and Douglas S Adams. Deployment analysis of the lenticular jointed antennas onboard the mars express spacecraft. *Journal of Spacecraft and Rockets*, 46 (2):394–402, 2009. ISSN 0022-4650.

[16] Mehran Mobrem, Lee Peterson, Velibor Cormarkovic, and Farzin Montazersadgh. An evaluation of structural analysis methodologies for space deployable structures. In *4th AIAA Spacecraft Structures Conference*, page 0851, 2017.

[17] NASA/JPL-Caltech, 2016. URL https://photojournal.jpl.nasa.gov/catalog/PIA20911.

[18] Nathan A Pehrson, Daniel C Ames, Samuel P Smith, Spencer P Magleby, and Manan

Arya. Self-deployable, self-stiffening, and retractable origami-based arrays for spacecraft. *AIAA Journal*, pages 1–8, 2020.

[19] S. Ragab and H Fayed. *Introduction to Finite Element Analysis for Engineers*. CRC Press, New York, 1st edition, 2017.

[20] Whitney D. Reynolds, Sungeun K. Jeon, Jeremy A. Banik, and Thomas W. Murphey. Advanced folding approaches for deployable spacecraft payloads. In *ASME 2013 International Design Engineering Technical Conferences and Computers and Information in Engineering Conference*, volume Volume 6B: 37th Mechanisms and Robotics Conference, V06BT07A043. doi: 10.1115/detc2013-13378. URL https://doi.org/10.1115/DETC2013-13378.

[21] M Salama, M Lou, and H Fang. Deployment of inflatable space structures-a review of recent developments. In *41st Structures, Structural Dynamics, and Materials Conference and Exhibit*, page 1730.

[22] Santosh Tiwari, Patrick Koch, Georges Fadel, and Kalyanmoy Deb. Amga: an archive-based micro genetic algorithm for multi-objective optimization. In *Proceedings of the 10th Annual Conference on Genetic and Evolutionary Computation*, pages 729–736, 2008.

[23] WD Wade, A Sinha, and R Singh. Study of wrap-rib antenna design. 1979.

[24] NASA/JPL/Corby Waste. URL http://www.fourth-millennium.net/mission-artwork/mars-express-MARSIS-antenna.html.

[25] J Jaap Wijker. *Spacecraft Structures*. Springer Science & Business Media, 2008.

[26] Edward L Wilson. Static and dynamic analysis of structures. *A Physical Approach with Emphasis on Earthquake Engineering*, 2004.

[27] James Winter, Greg Spanjers, D Cohen, Aaron Adler, Greg Ginet, Bronek Dichter, Jennifer Granata, K Denoyer, Thomas Murphey, Peter Wegner, et al. A proposed large deployable space structures experiment for high power, large aperture missions in meo. In *2004 IEEE Aerospace Conference Proceedings (IEEE Cat. No. 04TH8720)*, volume 1. IEEE, 2004.

[28] John J Zipay, Clarence T Modlin, and Curtis E Larsen. The ultimate factor of safety for aircraft and spacecraft-its history, applications and misconceptions. In *57th AIAA/ASCE/AHS/ASC Structures, Structural Dynamics, and Materials Conference*, page 1715, 2016.

Appendices

Appendix A

Matlab® Finite Element Analysis Code

```
le=L/ne; %Element length
R=18;    %Hub radius

%x(1) through x(ne) are thicknesses of each element
%x(1+ne)is tle elements' modulus of elasticity
%x(2+ne) is tle hinge torsional stiffness

%%Objective 1: Elastic energy stored in stowed hinge and
%fully wrapped panel

ElemE=0;
for i=1:ne
    Elem=0.5*(1/(R^2))*le*(x(ne+1)*H*((x(i))^3))/12;
    ElemE=Elem+ElemE;
end

PanelEE=ElemE;
```

```
18 HingeEE=0.5*((pi/2)^2)*x(ne+2);
19 Energy=PanelEE+HingeEE;
20
21 %% Natural Frequency FEA
22 k=[6,3*le,-6,3*le;3*le,2*(le^2),-3*le,le^2;-6,-3*le,6,-3*le;...
23         3*le,le^2,-3*le,2*(le^2)];
24 m=[156,22*le,54,-13*le;22*le,4*(le^2),13*le,-3*(le^2);...
25         54,13*le,156,-22*(le);-13*le,-3*(le^2),-22*le,4*(le^2)];
26
27 %Stiffness and Mass matricies of each element
28 for i=1:ne
29     Kelem(:,:,i)=((2*x(ne+1)*(H*((x(i))^3)))/(12*(le^3))).*k;
30     Melem(:,:,i)=((rho*x(i)*H*le)/420).*m;
31 end
32
33 %Assemble global stiffness matrix
34
35 K=zeros((ne*2)+2,(ne*2)+2);
36 for i=1:ne
37         Kk=zeros((ne*2)+2,(ne*2)+2);
38         j=((i*2)-1);
39
40         Kk(j,j)=Kelem(1,1,i);
41         Kk(j,j+1)=Kelem(1,2,i);
42         Kk(j,j+2)=Kelem(1,3,i);
```

```
43            Kk(j,j+3)=Kelem(1,4,i);
44            Kk(j+1,j)=Kelem(2,1,i);
45            Kk(j+1,j+1)=Kelem(2,2,i);
46            Kk(j+1,j+2)=Kelem(2,3,i);
47            Kk(j+1,j+3)=Kelem(2,4,i);
48            Kk(j+2,j)=Kelem(3,1,i);
49            Kk(j+2,j+1)=Kelem(3,2,i);
50            Kk(j+2,j+2)=Kelem(3,3,i);
51            Kk(j+2,j+3)=Kelem(3,4,i);
52            Kk(j+3,j)=Kelem(4,1,i);
53            Kk(j+3,j+1)=Kelem(4,2,i);
54            Kk(j+3,j+2)=Kelem(4,3,i);
55            Kk(j+3,j+3)=Kelem(4,4,i);
56
57            K=Kk+K;
58 end
59
60 %Assemble global mass matrix
61
62 M=zeros((ne*2)+2,(ne*2)+2);
63
64 for i=1:ne
65     Mm=zeros((ne*2)+2,(ne*2)+2);
66     j=(i*2)-1;
67
```

```
68            Mm(j,j)=Melem(1,1,i);
69            Mm(j,j+1)=Melem(1,2,i);
70            Mm(j,j+2)=Melem(1,3,i);
71            Mm(j,j+3)=Melem(1,4,i);
72            Mm(j+1,j)=Melem(2,1,i);
73            Mm(j+1,j+1)=Melem(2,2,i);
74            Mm(j+1,j+2)=Melem(2,3,i);
75            Mm(j+1,j+3)=Melem(2,4,i);
76            Mm(j+2,j)=Melem(3,1,i);
77            Mm(j+2,j+1)=Melem(3,2,i);
78            Mm(j+2,j+2)=Melem(3,3,i);
79            Mm(j+2,j+3)=Melem(3,4,i);
80            Mm(j+3,j)=Melem(4,1,i);
81            Mm(j+3,j+1)=Melem(4,2,i);
82            Mm(j+3,j+2)=Melem(4,3,i);
83            Mm(j+3,j+3)=Melem(4,4,i);
84
85            M=Mm+M;
86        end
87
88  %Boundary Conditions
89
90  %No shear at free end
91  %No moment at free end
92  %Linear spring at hinged end with stiffness= 1E7
```

```
93 %Hinge (rotational spring) stiffness= x(ne+2)
94
95 K(1,1)=K(1,1)+(1E7);
96 K(2,2)=K(2,2)+x(ne+2);
97
98 %% Objective 2: Natural frequency of panel
99
100 [eigvect,omega] = eig(K,M);
101
102 Freq = sqrt(diag(omega))/(2*pi);
103 Freq1=Freq(1);
104
105 OneOverFreq1=1/Freq1;
106 OneOverFreq1Sq=1/(Freq1^2);
107
108 %% Mass constraint
109
110 MTot=0;
111 for j=1:ne
112     M(j)=(L/ne)*H*rho*x(j);
113     MTot=MTot+M(j);
114 end
115
116 %% Stress constraint
117
```

```
118 St1=((x(1)*x(ne+1))/36);
119 St2=((x(2)*x(ne+1))/36);
120 St3=((x(3)*x(ne+1))/36);
121 St4=((x(4)*x(ne+1))/36);
122 St5=((x(5)*x(ne+1))/36);
123 St6=((x(6)*x(ne+1))/36);
124 St7=((x(7)*x(ne+1))/36);
125 St8=((x(8)*x(ne+1))/36);
126 St9=((x(9)*x(ne+1))/36);
127 St10=((x(10)*x(ne+1))/36);
128 St11=((x(11)*x(ne+1))/36);
129 St12=((x(12)*x(ne+1))/36);
130 St13=((x(13)*x(ne+1))/36);
131 St14=((x(14)*x(ne+1))/36);
132 St15=((x(15)*x(ne+1))/36);
133 St16=((x(16)*x(ne+1))/36);
134 St17=((x(17)*x(ne+1))/36);
135 St18=((x(18)*x(ne+1))/36);
136 St19=((x(19)*x(ne+1))/36);
137 St20=((x(20)*x(ne+1))/36);
138 St21=((x(21)*x(ne+1))/36);
139 St22=((x(22)*x(ne+1))/36);
140 St23=((x(23)*x(ne+1))/36);
141 St24=((x(24)*x(ne+1))/36);
142 St25=((x(25)*x(ne+1))/36);
```

```
143 St26=((x(26)*x(ne+1))/36);
144 St27=((x(27)*x(ne+1))/36);
145 St28=((x(28)*x(ne+1))/36);
146 St29=((x(29)*x(ne+1))/36);
147 St30=((x(30)*x(ne+1))/36);
148 St31=((x(31)*x(ne+1))/36);
149 St32=((x(32)*x(ne+1))/36);
150 St33=((x(33)*x(ne+1))/36);
151 St34=((x(34)*x(ne+1))/36);
152 St35=((x(35)*x(ne+1))/36);
153 St36=((x(36)*x(ne+1))/36);
154 St37=((x(37)*x(ne+1))/36);
155 St38=((x(38)*x(ne+1))/36);
156 St39=((x(39)*x(ne+1))/36);
157 St40=((x(40)*x(ne+1))/36);
```